Optimization of large-scale fabrication of dielectric elastomer transducers

Hassouneh, Suzan Sager

Publication date:
2015

Document Version
Publisher's PDF, also known as Version of record

Optimization of large-scale fabrication of dielectric elastomer transducers

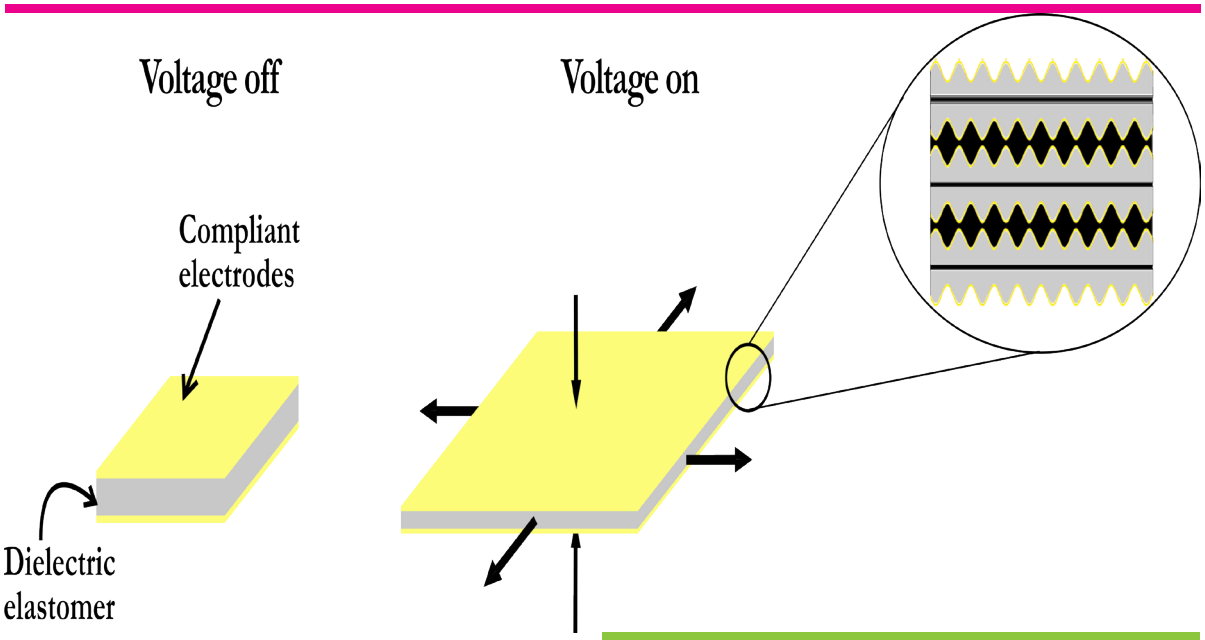

Suzan Sager Hassouneh
Ph.D. Thesis
February 2015

DTU Chemical Engineering
Department of Chemical and Biochemical Engineering

Optimization of large-scale fabrication of dielectric elastomer transducers

Suzan Sager Hassouneh
Ph.D. Thesis
February 2015

DTU Chemical Engineering
Department of Chemical and Biochemical Engineering

Address: The Danish Polymer Centre
Department of Chemical and Biochemical Engineering
Technical University of Denmark
Building 227
DK-2800 Kgs. Lyngby
Denmark
Phone: +45 4525 6801
Web: www.dpc.kt.dtu.dk

Print: J&R Frydenberg A/S
København
Juli 2015

ISBN: 978-87-93054-75-2

Preface

The work presented herein is the result of my Ph.D. study, carried out at the Danish Polymer Centre (DPC), Department of Chemical and Biochemical Engineering, Technical University of Denmark (DTU), between August 1st 2012 and February 27th 2015. The project was funded by InnovationsFonden.

Firstly, I would like to thank my main supervisor, Anne Ladegaard Skov, for believing in me and granting me this opportunity. I will be forever grateful for your endless support, guidance and encouragement. Your friendly approach and ability to see the bigger picture, as well as always having time to discuss whatever, were very much appreciated.

Secondly, I owe gratitude to my co-supervisor, Anders Egede Daugaard, for his great advice. You joined the project halfway through, and your experience and knowledge were invaluable.

A big thank you goes out to our collaborators at Danfoss Polypower A/S for their knowledge and guidance throughout the project.

I would also like to thank my colleagues at DPC for the great working environment and social gatherings. Especially, Frederikke Bahrt Madsen is thanked for her help and advice concerning the writing of this thesis.

Finally, I owe a great debt of gratitude to my family for always standing by me and for all their love and support. I also thank my friends, Amnah, Hanan and Nawal, for their support and encouragement whenever needed.

Kgs. Lyngby, February 2015

Suzan Sager Hassouneh

Abstract

Dielectric elastomers (DEs) have gained substantial ground in many different applications, such as wave energy harvesting, valves and loudspeakers. For DE technology to be commercially viable, it is necessary that any large-scale production operation is non-destructive, efficient and cheap.

Danfoss Polypower A/S employs a large-scale process for manufacturing DE films with one-sided corrugated surfaces. The DEs are manufactured by coating an elastomer mixture to a corrugated carrier web, thereby imprinting the corrugations onto the elastomer. The corrugated elastomer is then sputtered with metal electrodes on the corrugated surface, and due to these corrugated surfaces the metal electrodes maintain conductivities up to more than 100% strain of the elastomer film. The films are then laminated in multiple layers to fabricate DE transducers. However, the current manufacturing process is not trouble-free, and two issues in particular have great influence on the performance of DE transducers. The first issue is the release of the corrugated elastomer film from the carrier web, due to the large surface area and flexible nature of the elastomer film, while the second issue relates to the lamination of DE films. Currently, the films are contacted without adhesion, in order to yield double-sided corrugations, which in turn causes friction between the layers and thus reduces the lifespan of the transducer. Furthermore, air can be trapped in the interface, thereby causing a decrease in electrical breakdown strength. Other issues may also arise, depending on how the elements are assembled.

This thesis is based on optimising the large-scale manufacture of DE transducers. The hot embossing technology is used to impart corrugations onto elastomer film surfaces. Embossing, which was performed for samples with different r-values, showed that the process was applicable for different hardnesses of the material, while time intervals for the different materials were also determined.

An attempt to solve the lamination issue was made by applying stronger adhesion methods when preparing monolithic elements. Due to the corrugations, the films were able to adhere in different configurations (back-to-back, front-to-back and front-to-front). The first approach involved adhering PDMS to PDMS (back-to-back), for which two routes were followed. The first route involved using an aminosilane as an adhesion agent after modifying the PDMS surface through plasma treatment, which demonstrated that the

laminates were slightly stiffer and more fragile in respect to tearing. The other route involved modifying the surfaces through plasma treatment and by adhering the layers, which showed to be a suitable method and allowed high-strength laminates to perform as monolithic elements.

For the front-to-back and front-to-front configurations, conductive elastomers were utilised. One approach involved adding the cheap and conductive filler, exfoliated graphite (EG) to a PDMS matrix to increase dielectric permittivity. The results showed that even at low concentrations, EG influenced the overall performance of the reinforced elastomer matrix, indicating that increasing the concentration further to make conductive elastomers would compromise the elastic nature of the elastomer due to large EG dimensions; consequently, EG-based elastomers as conductive adhesives were rejected. Dielectric properties below the percolation threshold were subsequently investigated, in order to conclude the study.

In order to avoid destroying the network structure, carbon nanotubes (CNTs) were used as fillers during the preparation of the conductive elastomers and as received CNTs and modified CNTs were investigated. The unmodified CNTs were mixed with an ionic liquid, and two dispersion methods were investigated. The first method involved the ultrasonication of CNT/IL, which showed that conductivity increased in line with increasing CNT at concentrations lower than 5 wt% when CNTs were mixed with IL. The second method involved roll milling the composite, which decreased conductivity when concentrations exceeded 4 wt% for the CNT/IL composites. However, the obtained conductivities were increased for similar concentrations by roll milling.

The modified CNTs were grafted covalently to the CNT surface with poly(methacryloyl polydimethylsiloxane), resulting in the obtained conductivities being comparable to commercially available Elastosil LR3162, even at low functionalisation.

The optimized methods allow new processes for the production of DE film with corrugations and efficient DE transducers.

Resumé på dansk

Dielektriske elastomere har vundet betydelig indpas i mange forskellige applikationer, såsom bølgehøstere, ventiler og højtalere. For at gøre DE teknologien kommercielt levedygtig, er det nødvendigt at enhver stor skala produktion er ikke-destruktiv, effektiv og billig. En stor aktør i produktionen af DE film er Danfoss Polypower A/S, som producerer DE film med ensidige korrugerede overflader. Filmene bliver fremstillet ved at coate en flydende elastomer blanding på en korrugeret carrierweb, hvorved elastomeren bliver præget med korrugeringerne, når filmen hærder. Elastomer filmen aftages carrierweb'en og metal elektroder bliver derefter påført den korrugerede overflade og på grund af disse korrugerede overflader kan metal elektroderne opretholde ledningsevner ved mere end 100% stræk af elastomer filmene. Filmene lamineres derefter i flere lag til fremstilling af DE transducere. Den nuværende fremstillingsproces er dog ikke problemfri og to problemstillinger har i særdeleshed stor indflydelse på ydeevnen af DE transducere. Den første problemstilling er aftagelsen af de korrugerede DE film fra carrierweb'en, grundet det store overfladeareal og elastomer filmens fleksible natur, mens den anden problemstilling relaterer til lamineringen af DE filmene. I øjeblikket lamineres filmene uden adhæsion, med henblik på at give dobbeltsidet korrugeringer, hvilket forårsager friktion mellem lagene og således reducerer levetiden af transduceren. Endvidere kan luft blive fanget i grænsefladen, hvorved et fald i elektrisk sammenbrudstyrke forekommer. Andre problemer kan også opstå, afhængigt af hvordan elementerne er samlet.

Nærværende afhandling er baseret på at optimere fremstillingen af DE transducere i stor skala. Først er hot embossing (varmeprægning) teknologien er forsøgt anvendt til at præge elastomer filmens overflader med korrugeringer. Prægningen er foretaget på prøver med forskellige r-værdier og viste at metoden var anvendelig for forskellige hårdheder af materialet, mens tidsintervallerne for de forskellige materialer også blev bestemt.

Et forsøg på at løse problemstillingen angående lamineringen var gjort ved at anvende stærkere vedhæftningsmetoder til udarbejdelsen af monolitiske elementer. På grund af korrugeringerne er det muligt at vedhæfte filmene i forskellige konfigurationer. Den første strategi omfattede klæbning as PDMS til PDMS i en bagside-til-bagside konfiguration. PDMS overfladerne blev modificeret ved plasma behandling og det viste sig at være en

egnet metode til fremstilling af høj-styrke laminater der optræder som monolitiske elementer.

Ledende elastomere blev udnyttet til vedhæftning af DE film i front-til-bagside og front-til-front konfigurationerne. En fremgangsmåde involverede tilsætningen af det billige ledende fyldstof, ekspanderet grafit (EG) til PDMS matricen. Resultaterne viste at selv ved lave koncentrationer, påvirkede EG den overordnede ydeevne af den forstærkede elastomer matrix, hvilket indikerede at en yderligere forøgelse af EG-koncentrationen vil kompromittere elastomerens elastiske karakter, grundet EGs store størrelse. Derfor ble EG-baserede elastomere afvist som ledende klæbere. De dielektriske egenskaber under perkolation grænsen blev efterfølgende undersøgt med henblik på at afslutte undersøgelsen. For at undgå at ødelægge netværkstrukturen blev kulstof nanorør anvendt som fyldstoffer til fremstilling af ledende elastomerer. Både modificerede og ikke-modificerede nanorør blev undersøgt. De ikke-modificerede nanorør blev blandet med en ioniske væske og to dispergeringsmetoder blev undersøgt. I den første metodeblev nanorør og ioniske væske dispergerede ved ultrasonikering, som viste at ledningsevnen steg i takt med stigende nanorør koncentration for koncentrationer lavere end 5 vægt%. I den anden metode blev dispergeringen foretaget ved en roll mill (valsemølle). Prøverne viste et fald i ledningsevne når koncentrationen oversteg 4 vægt% for nanorør/ionisk væske kompositterne. Ledningsevnen steg med stigende nanorør koncentration for prøverne uden ionisk væske. De opnåede ledningsevner ved givne koncentrationer blev øget ved valseformaling, sammenlignet med ultrasonikeringsmetoden.

Poly(methacryloyl polydimetylsiloxan) blev kovalent bundet til nanorørenes overflade, hvilket resulterede i opnåede ledningsevner, der var sammenlignelige med den kommercielt tilgængelige Elastosil LR3162, selv ved lav funktionaliseringsgrad.

De optimerede metoder muliggør nye processer til fremstilling af DE film med korrugeringer og effektive DE transducere.

Table of contents

Abbreviations and symbols

AIBN	Azobisisobutyronitrile
AgNW	Silver nanowires
B2B	Back-to-back
CNT	Carbon nanotubes
CP	Conductive polymers
DE	Dielectric elastomer
DPP	Danfoss Polypower A/S
ε'	Dielectric permittivity
ε"	Dielectric loss
EAP	Electro active polymers
E_B	Electrical breakdown strength
F2B	Front-to-back
F2F	Front-to-front
f-CNTs	Functionalized carbon nanotubes
G'	Storage modulus
G"	Loss modulus
IL	Ionic liquid
LR	Liquid rubber
MW	Multiwall
PANI	Polyaniline
PEDOT	Poly(3,4-ethylenedioxythiophene)
PDMS	Polydimethylsiloxane
PU	Polyurethane
RT	Room temperature
SEM	Scanning electron microscope
σ	Conductivity
SW	Single wall
Tan δ	Loss tangent
wt%	Weight percent
Y	Young's modulus

Thesis structure

Objectives

The objective of this thesis is to develop tools that will improve the manufacture of dielectric elastomer (DE) transducers on an industrial scale. Several methods for manufacturing DE transducers are applicable, one of which involves is to coat a liquid elastomer mixture to a corrugated carrier web and cures directly on the carrier web. The elastomer film is then de-laminated from the carrier web and the corrugations are imprinted on the elastomer film, before metal electrodes are sputtered on the corrugated surface. DE transducers are assembled by adding together multiple layers and connecting them to electrical wires via a supporting structure. Optimisation of the present process is needed, and this thesis focuses on two parts of the process.

The focus in the first part falls on an alternative method for preparing corrugated PDMS film. This issue is addressed by using a hot-embossing method to imprint structures onto the elastomer film.

The focus in the second part involves preparing monolithic structures by adhering DE films in multiple layers, in order to increase the energy density and robustness of the DE transducers. The films can be adhered in different configurations, due to the design of the DE films and the requirements of the adhesive for the different configurations varies. Adhesives for the different configurations are investigated in this thesis.

Outline

The field of dielectric elastomers is introduced in Chapter 1, where the relevant issues for this thesis are addressed. Chapter 2 deals with an alternative method to imprint corrugation on DE films, where hot-embossing technology commonly used for thermoplasts is used. Chapter 3 then focuses on the back-to-back (B2B) configuration, where DE films are plasma-treated to modify the surfaces and to enable the adhesion of the films. Work on adding exfoliated graphite as a filler in PDMS, as well as the properties of the material, is presented in Chapter 4, while Chapter 5 deals with dispersing carbon nanotubes (CNTs) in PDMS in order to fabricate conductive elastomers to be used as adhesive in the front-to-back (F2B) and front-to-front (F2F) configurations. A conclusion and an overview of

future work can be found in Chapter 6, and experimental procedures can be found in Chapter 7.

The work presented herein resulted in an article published in the Danish journal *Dansk Kemi* (in Danish) and an article published in *Macromolecular Material and Engineering*. Two additional articles are to be submitted.

Appendix A:

S. Hassouneh, S. Vudayagiri, L. Yu, M. Junker, U.Hansen and A. L. Skov, 2012, Fremstilling af dielektriske elektroaktive polymerer i stor skala, *Dansk Kemi*, **93** (10), 22-24.

Appendix B:

S. S. Hassouneh, A. E. Daugaard, A. L. Skov, 2015, Design of elastomer structure to facilitate incorporation of expanded graphite in silicones without compromising electromechanical integrity, *Macromolecular Materials and Engineering,* **300** (5), 542-550

Other publications (not included in the thesis):

A. E. Daugaard, S. S. Hassouneh, M. Kostrzewska, A. C. Bejenariu, A. L. Skov, 2013, High dielectric permittivity elastomers from well-dispersed expanded graphite in low concentrations, *Proceeding of SPIE*, **8687**, 868729-1 – 868729-11

S. Vudayagiri, L. Yu, S. S. Hassouneh, A. L. Skov, 2013, Hot-embossing of microstructures on addition-curing polydimethylsiloxane films, *Proceedings of SPIE*, **8687**, 86870S-1 – 86870S-16.

S. Vudayagiri, L. Yu, S. S. Hassouneh, A. L. Skov, 2014, Hot embossing of microstructures on addition curing polydimethylsiloxane films, *Journal of Elastomers and Plastics*, **46** (7), 623-643.

S. Vudayagiri, S. Zakaria, L. Yu, S. S. Hassouneh, M. Benslimane, A. L. Skov, 2014, High breakdown-strength composites from liquid silicone rubbers, *Smart Materials and Structures*, **23** (10), 105017.

S. Vudayagiri, L. Yu, S. S. Hassouneh, U. Hansen, A. L. Skov, 2015, Bilaterally microstructured thin polydimethylsiloxane film production, *Polymer-Plastics Technology and Engineering*, **54** (4), 425-432.

1. Introduction

Interest in the use of polymers for different applications has increased due to attractive characteristics such as being lightweight, flexible and low in cost. Polymers also have the advantage that they can be tailored to fit specific requirements. One class of polymers that has attracted a good deal of attention for the last two decades is responsive polymers, which is a subcategory of "smart materials." Responsive polymers may exhibit changes in size and shape, in response to external stimuli such as chemical, optical, thermal, magnetic or electrical[1–3]. Electroactive polymers (EAPs) are responsive polymers that are activated by an electrical field and can be used as transducers such as actuators, generators and sensors. Actuators convert electrical energy into mechanical energy, and when voltage is applied to the electrodes the EAP material contracts in thickness and expands in area, due to electrostatic forces. The reverse working principle is applicable for generators, whereby mechanical energy is converted into electrical energy. An electrical field is applied to stretched EAP material, and when the film relaxes, the thickness increases and the elastic stresses in the film work against the electrical field pressure, which then makes the voltage increase significantly. When an external force or pressure is applied to an EAP with an applied voltage, the material de-forms, which leads to a measurable change in capacitance that, ultimately, can be utilised for sensing.

EAPs are arranged into two major groups, namely ionic and the electronic. Ionic EAPs actuate through the diffusion of ions as a response to an electrical field and are further divided into subgroups, such as carbon nanotubes (CNTs)[4], conductive polymers (CPs)[5–7] and ionic polymer-metal composites (IPMCs)[8,9]. Driving voltages can be as low as 1-2 V, but ionic EAPs require the use of electrolytes, and therefore encapsulation or a protective layer are needed to operate in open-air conditions. Electronic EAPs activate by shifting electrical charges[1] and can also be divided into subgroups, such as liquid crystal elastomers, ferroelectric polymers and dielectric elastomers (DEs). The advantage of DEs is their fast response time, usually in the order of milliseconds, large actuation forces and high mechanical energy density, all of which make these materials interesting[2].

DEs consist of an elastomer film, sandwiched between compliant electrodes on both sides and connected to an electrical circuit. As a consequence of the incompressible nature of the

elastomer, the elastomer film compresses in thickness and expands in the planar direction when a voltage is applied to the electrodes, as illustrated in Figure 1[3,10].

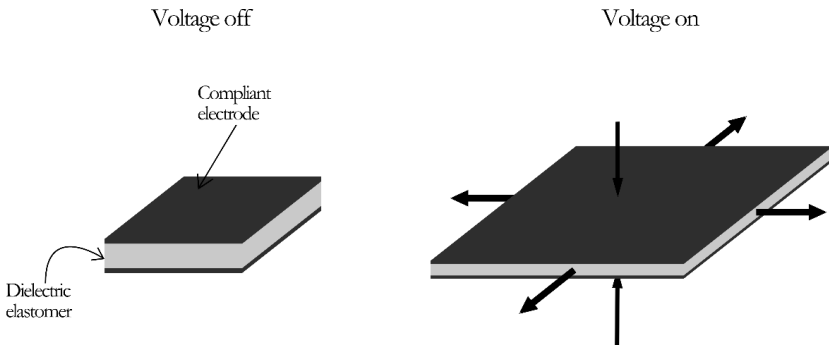

Figure 1 The working principle of DE transducers. The DE elastomer is sandwiched between compliant electrodes, and by applying voltage the DE elastomer contracts in thickness and expands in area, due to electrostatic forces between the electrodes.

This deformation is the result of electrostatic forces between two electrodes with opposite electrical charges, whereby opposite charges attract each other and similar charges are separated. The induced strain at a given electrical field has two contributions, namely electrostatic (Maxwell pressure) and electrostrictive pressure. The electrostatic response for DEs is derived by Pelrine et al.[3] and is expressed by

$$p_{Maxwell} = -\frac{\varepsilon_0 \cdot \varepsilon_r \cdot E^2}{Y} = -\frac{\varepsilon_0 \cdot \varepsilon_r}{Y} \cdot \left(\frac{U}{d}\right)^2 \quad (1)$$

where $p_{Maxwell}$ is the Maxwell strain, Y is the Young's modulus, ε_0 vacuum permittivity, ε_r relative dielectric permittivity, E the electrical field, U applied voltage and d the original thickness of the material. Maxwell pressure arises due to a change in distribution inside the elastomer with strain. Amorphous polymers are only affected by the Maxwell pressure when actuated.

The Young's modulus is a measure of a material's elasticity (stiffness). Due to the incompressible nature of silicones the Young's modulus can be determined by Y=3*G, where G is the shear modulus and can be expressed as the shear storage modulus (G') at very small frequencies ($G=G'(\omega) \rightarrow 0$). The shear storage modulus and the shear loss modulus (G") can be obtained through linear shear rheology, whereby a sample is sheared at a given strain at different frequencies.

Dielectric permittivity describes a material's ability to store electrical energy. However, to utilise the stored electrical energy the dielectric losses, ε", must be as low as possible in order not to generate heat exceeding natural thermal conduction, which ultimately will lead to thermal breakdown [11].

The material properties expressed in Eq. 1 are not the only properties that influence the overall performance of an elastomer; one important property is electrical breakdown strength, E_B, which is the applied voltage at which a material of a given thickness breaks down. E_B is desired to be as high as possible, and several parameters influence E_B such as a material's temperature and structure as well as impurities in/on the material.

1.1 Materials

Several materials have been investigated as DE materials, such as acrylics[3,12,13], polyurethanes (PUs)[14–16], polybutadienes[17,18], flouroelastomers[19] and silicones[20–24]. Furthermore, a lot of research has focused on acrylics and silicones, due to their superior actuator performance, when no pre-stretch is utilised, and their excellent elastic and electroactive properties[1,10,25–27].

The acrylic adhesive (VHB) produced by 3M is the most explored acrylic for DEs, because it has large actuation strains (380%), electromechanical conversion efficiency (60 - 90%) and a high elastic energy conversion rate (3.4 J/s)[2,3,13,28,29]. The material is subjected to significant uniaxial or biaxial pre-strain to achieve these performances. The disadvantage of pre-straining the film is that elastomer stress relaxes, thereby leading to poor product lifespan. Furthermore, a supporting structure is used to keep the film pre-strained, which adds weight to the final actuator as well as instability at the interface between the material and the supporting structure [30].

Polydimethylsiloxane (PDMS) has gained a good deal of interest due to fast responses, high efficiency and stability over a wide temperature range. The disadvantage of PDMS in comparison to acrylics is its relatively low dielectric constant, which means that it requires higher working voltages for a given strain and Young's modulus.

The commercially available elastomers used for DEs have not been developed for this specific purpose, so intensive research has focused on optimising the properties of the materials. Eq. 1 can be used as basis for improving mechanical and dielectric properties. A critical parameter is working voltage, which should be reduced because there are a number

of dangers associated with the use of high voltages. Furthermore, applicability will be limited, since expensive electronics are required. According to Eq. 1, the greatest reduction in voltage is achieved by reducing elastomer thickness; however, film thicknesses are reduced to such an extent that producing thinner films on an industrial scale will cause processing issues[31]. Moreover, handling thinner films can be difficult, since they may not withstand peel forces and will subsequently tear. Another approach would be to decrease the Young's modulus, making the elastomer softer; however, decreasing Y will decrease electrical breakdown strength and lead to premature failure[32]. Working voltage could be reduced by increasing relative dielectric permittivity, which will facilitate better energy storage in the material.

A way to improve the dielectric constant is to add fillers to the matrix, such as the metal oxide fillers TiO_2[22,24,33–40], $BaTiO_3$[38,40–42] and Al_2O_3[38]. The disadvantage of these composite systems is an increase in the Young's modulus as well as in dielectric losses. Furthermore, fillers have a tendency to agglomerate, which will decrease electrical breakdown strength.

Another approach to increasing the dielectric constant, without changing mechanical properties, is to graft dipolar groups to either the crosslinking site [43–45] or the elastomer backbone[46,47]. Increasing the content of crosslinking sites is limited by the mechanical properties, since an excess amount of crosslinker will lead to dangling ends. Grafting the dipolar groups to the backbone also has disadvantages, since molecular weight cannot be controlled and this could lead to stiffer elastomer. These developed materials still need optimisation to make effective DE transducers and to commercialise the technology. Furthermore, dielectric material is not the only material to influence DE transducers, as electrodes are another important aspect of DEs. These electrodes are submitted to the same strain as the dielectric layer, which is why it is crucial that they are compliant to avoid premature failure. Additionally, the electrodes should remain conductive when sustaining deformation. Precious metals can be used as electrodes due to their high conductivity ranges; however, metal electrodes are not stretchable, so in order to utilise precious metals as electrodes, corrugated dielectric films are necessary, because they will enable significant strain and facilitate the use of metals as compliant electrodes.

The properties described in the previous sections are typical parameters governing the actuation capability of DEs. However, an industrial-scale production process places additional conditions on the materials, all of which will be discussed in the following.

1.2 Large-scale production

Danfoss Polypower A/S (DPP) is one of the very few producers of DEs worldwide, due to the lack of any form of explicit business potential. DPP uses PDMS as an elastomer material, and the manufacturing process will be described in the following section.

The manufacturing process is performed in a clean room in which temperature and humidity are controlled, in order to minimise defects on the manufactured elastomers caused by contamination. The elastomer batch is prepared by thoroughly mixing the PDMS, the desired fillers, an inhibitor and a solvent using a speedmixer and a roll mill. An inhibitor is added to the mixture to postpone the curing, and the solvent is used to achieve the desired viscosity of the mixture, in order to ease the coating process.

The thoroughly mixed liquid elastomer batch is then coated on a corrugated carrier web, which are long liners with microscale sinusoidal corrugations with a 10 μm period and a depth of 5 μm. Another design, at 7 μm in both period and depth, is also used. The direction of the corrugation can be parallel to the length of the web (down-web) or parallel to the width of the web (cross-web)[48,49], and the carrier web is used as a mould to impart the microstructures onto the elastomer film. The coating process is a conventional roll-to-roll manufacturing process, as illustrated in Figure 2.

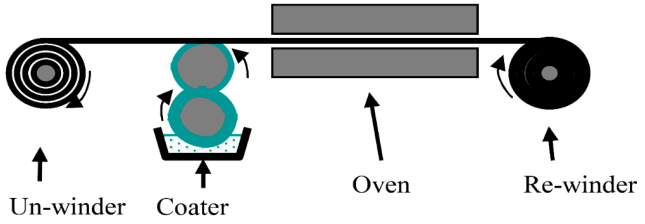

Figure 2 The roll-2-roll process for fabricating DE film at DPP. The liquid elastomer is coated on the carrier web using a gravure coater. The thin elastomer film cures in the oven and is rewound onto rolls after curing[48].

The carrier web is unwound from a roll and the liquid elastomer mixture is coated uniformly as a thin film (~ 40 μm) on the carrier web, using a gravure coater. The elastomer is then run through an oven, to speed up the curing process, and the elastomer is formed. PDMS elastomers are formed by a hydrosilylation reaction, where vinyl groups react with hydride groups in the presence of a platinum catalyst, and where the double

bond in the vinyl is broken and the network is formed. The reaction mechanism is illustrated in Figure 3.

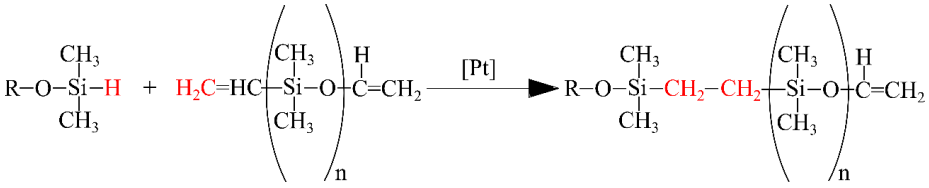

Figure 3 The hydrosilylation reaction. Vinyl groups react with hydride groups in the presence of a platinum catalyst.

In order to obtain a better overview of how the network is formed from crosslinking PDMS with a 4-functional (4f) crosslinker, a schematic illustration of the above reaction is shown in Figure 4.

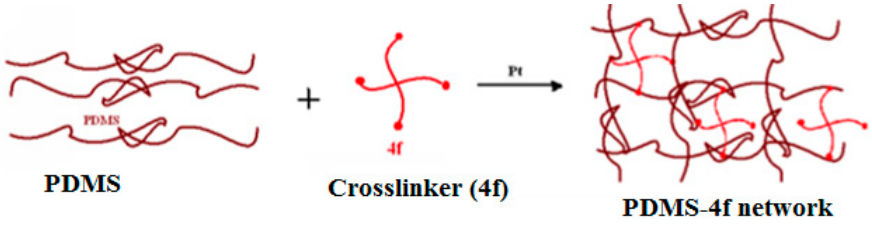

Figure 4 A schematic illustration of network formation between PDMS and a 4-functional crosslinker.

When the elastomer film is fully cured, it is de-laminated from the carrier web by using a controlled automated machine, and the flat surface is then placed on backing material with the corrugation facing upwards. The backing material is used as a supportive layer to ease the rolling and storage of films, in order to avoid the films sticking to each other.

A roll-to-roll vacuum sputtering process is used to add electrodes onto the elastomer film, and the process is divided into three zones, as illustrated in Figure 5.

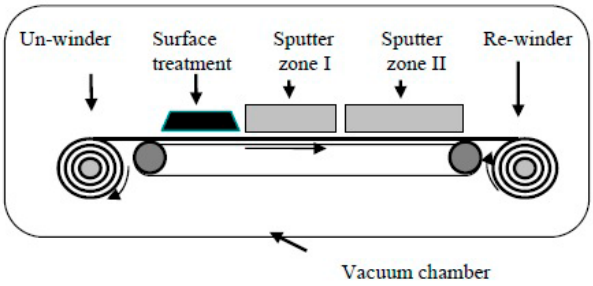

Figure 5 The metal sputtering of electrodes on the corrugated surface of DPP films. Electrode sputtering is divided into three zones. The first involves plasma-treating the surface and the second and third zones involve electrode sputtering at low and high rates, respectively[48].

In the first zone, the film is plasma-treated (in a vacuum) to improve adhesion properties. In the second zone, the electrode material is sputtered at a low rate to seed the corrugated surface of the film. The electrode material employed in this process is silver, but gold and nickel can also be used[48]. In the third zone, the electrode is sputtered at a higher sputtering rate to increase the manufacturing flow. Electrode thickness is 10 nm [48].

The metallised films are laminated in a back-to-back (B2B) or front-to-back (F2B) configuration (see Figure 6) using custom-built lamination equipment, at which point the surfaces come into contact. The B2B configuration means that the non-metallised sides of two films are contacted, while for the F2B configuration the metallised side of one film faces the non-metallised of the second film. The Front-to-Front (F2F) configuration involves the metallised sides of two films adhered together. The laminates can then be rolled, stacked or folded to prepare different transducers.

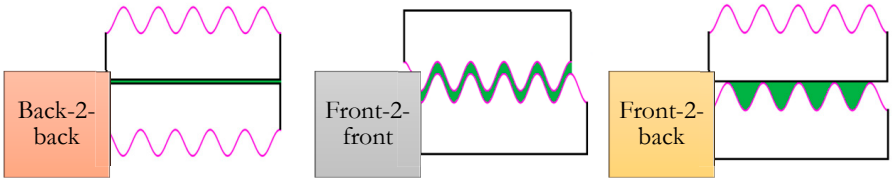

Figure 6 Different configurations for film adhesion. In the back-to-back configuration the flat sides are adhered together. The corrugated sides are adhered together in the front-to-front configuration and for the front-to-back configuration a corrugated side is adhered with a flat side. Green colouration above indicates the adhesive used for the different configurations.

A number of challenges need to be overcome in the process described above. One such issue is the release of the elastomer film from the carrier web. De-laminating the elastomer film from the carrier web is complicated, due to the large surface area between the carrier web and the elastomer, and the de-lamination induces pre-strain in the film that subsequently affects the performance of the films[31].

Vudayagiri et al.[50] showed that pre-coating the carrier web with a non-ionic surfactant lowered the peel forces of the elastomer film, without influencing the Young's modulus or the dielectric constant.

Another challenge is lamination without applying adhesive to the metallised films, as the disadvantage of this method is air bubbles or dust particles becoming trapped in the interface, which will make the laminate vulnerable to breakdown. Furthermore, when layers are laminated without adhesive, they are mechanically independent, which will cause friction between the layers during operation and subsequently reduce the lifetime of the element.

1.3 Monolithic structures

Fabrication of DE transducers with multiple layers is favourable, since transducers will become more robust and ultimately prolong the lifetime of the transducer. Furthermore, a dielectric elastomer film has a given energy density, and by adding multiple layers to an element, the energy density of the element increases, since the supporting structure is relatively heavy. To eliminate friction, as well as air bubbles and dust, the layers are adhered together, thereby making a monolithic structured DE transducer.

The requirements for the adhesives vary according to different configurations. For the B2B configuration, for instance, the adhesive should bond PDMS with PDMS. Furthermore, the adhesive should be insulating and as a minimum prerequisite have the same dielectric properties as the DEs, in order not to break down before the DEs. Another requirement is that the mechanical properties should be equal to the DEs, since a stiffer interface will cause a reduction in actuation. If the material is softer, E_B will decrease and subsequently lead to premature failure [32].

Monolithic configurations, such as helical and folded configurations, where insulating material is used adhesive have been investigated[51,52]. The helical actuator is composed of two helices, one coated with compliant electrodes and one smeared with uncured dielectric material. The two helices are coupled so that the electrodes and the DE alternate. The

coupled helices are placed in a mould containing uncured dielectric material, and the element is kept in the mould for 12 hours at room temperature until the dielectric material is cured. The dielectric material works as an insulating material to prevent air discharge during actuation [51].

A folded actuator consists of a continuous strip of elastomer coated with compliant electrodes, folded and sealed with a thin coating of the same elastomer material. The folded and helical structures are fabricated at thicknesses of between 0.5 and 0.8 mm for each layer. These thicknesses, as well as the thin coating used as insulation, require higher working voltages and result in an increase in mechanical resistance[51,52].

For the F2F configuration, the adhesive should be conductive, since adding an insulating adhesive will make the elements resemble the F2B configuration. Conductive elastomers can be used as adhesive between the layers as well as a link between the DEs and the electrical connection. In the F2F configuration, the conductive elastomer should adhere to the metal electrodes, and adhesion strength should be sufficient to avoid de-lamination during operation. The mechanical properties of the conductive elastomer depend on the application; for adhesion between the layers, for instance, the conductive elastomer should have the same mechanical properties as the DE layer, so that actuation is not reduced. However, if the conductive elastomer is used as an adhesive between the DEs and the electrical connection, the adhesive can be stiffer, to gain a better transition from the soft DEs to the very stiff electrical connection.

Adhesive in the F2B configuration should be able to adhere the metal electrodes to the PDMS and should have – as the other two configurations – the same mechanical properties as the DE layers. Furthermore, the adhesive can be either insulating or conductive, and the dielectric or electrical properties should be the same as the adhesives for the B2B and F2F configurations, respectively.

Adhering multiple layers together is a commonly used practice in the fabrication of microfluidic devices and micro electro mechanical systems (MEMS), and different approaches have been investigated for these systems[53,54]. One approach in relation to silicone dielectric elastomers is to use a sticky layer containing a deficient amount of crosslinker, which enables direct bonding to another surface with excess crosslinker[55]. The disadvantage of this method, however, is that the layers most likely possess different mechanical and electrical properties, which will influence the overall performance of the transducer. A second approach is to add uncured PDMS or crosslinker as glue between the

layers[56–58]. The addition of PDMS as glue increases the thickness of the dielectric material, which in turn, according to Eq. 1, reduces the actuation strain. A third approach is to plasma-treat the PDMS films, which is illustrated in Figure 7. Through this approach the Si-CH_3 groups on the surface of the elastomer are modified to silanol groups (Si-OH), and when films are brought together covalent siloxane bonds (Si-O-Si) are formed in the interface[53].

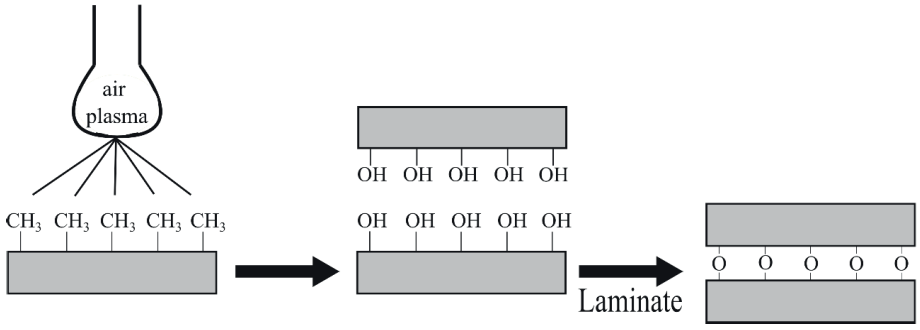

Figure 7 Plasma-treatment of PDMS films. The surface is modified from Si-CH_3 to Si-OH, and by laminating the films covalent bonds are formed.

A variety of gases, such as argon, carbondioxide, oxygen and air, can be used to create plasma[59,60], but for all gases, the plasma is produced in a low-vacuum environment, which is extremely expensive in industrial processes.

1.4 Conductive elastomers

Conductive elastomers have gained a good deal of interest over the last few decades, and a lot of research in this area has focused on using conductive elastomers as compliant electrodes for DE transducers, due to the flexible nature of conductive elastomers. The conductive elastomer must be able to sustain large deformation while remaining conductive and still being able to withstand millions of cycles[61]. Furthermore, conductive elastomers can be used as adhesive between layers (F2F) as well as interconnections between the DE films and the electronic components of the transducer. Several methods have been used to prepare conductive elastomers, such as grafting conductive polymers to soft block copolymers[62], blending conductive polymers with elastomers[63] or fabricating stretchable conductors from bacterial cellulose[64]. The preparation of these

conductive elastomers is either tedious and/or requires a lot of solvent, which is not preferable from an industrial point of view.

Another way to prepare conductive elastomers is to add conductive fillers to an insulating elastomer above the percolation threshold at which the material becomes conductive. Various fillers have been used in this respect, such as silver nanowires (AgNWs), exfoliated graphite (EG) and carbon nanotubes (CNTs).

AgNWs are synthesised through the reduction of silver nitrate in the presence of polyvinylpyrrolidone in ethylene glycol[65,66], which means that the AgNWs are in suspension. The conductivity of conductive elastomers prepared by adding AgNWs as fillers has been shown to decrease when the elastomer is strained[67,68].

CNTs, which have garnered much attention because of their excellent mechanical, thermal and electrical properties[69,70], are single or multiple graphene layers rolled into cylinders. The graphene layers consist of hexagonally arranged carbon-carbon bonds. To close the graphitic hexagonal network carbon atoms at the endcaps are placed into both hexagons and pentagons[71,72]. CNTs are distinguished by the number of sheets they consist of and are specified as single-walled (SW) and multi-walled (MW) [73–75].

CNTs are preferred as nanofillers for conductive elastomers, since conducting networks are achieved at low concentrations, due to their high aspect ratio[70,74].

However, a drawback of CNTs is their poor dispersion in elastomers, due to the formation of agglomerates as a result of the van der Waals force of interaction between the CNTs[76,77]. In order to achieve the better dispersion of CNTs in elastomer, covalent and non-covalent modifications can be used. Covalent modification includes, amongst others, grafting functionality to the CNT surface[78–80], while non-covalent modification can involve mixing with ionic liquids (ILs), which are liquids at room temperature that consist of ions. They are either a mix of an organic-inorganic salt or a purely organic salt and can be tailored to specific properties based on the choice of cations and anions, examples of which are depicted in Figure 8.

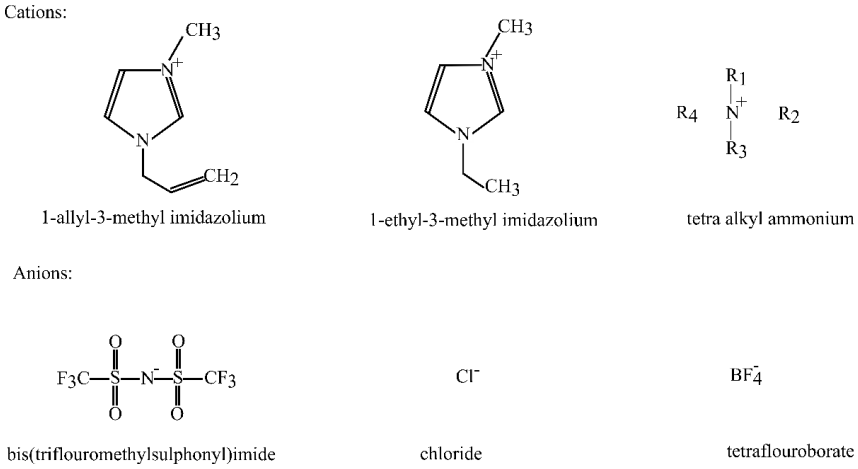

Figure 8 Examples of anionic and cationic constituents for ILs. The ILs can be tailored to specific properties.

The use of ILs was found to improve the dispersion of CNT, and in particular the imidazolium type IL demonstrates an increase in the conductivity of the composite[75,81–89]. Many different types of conductive elastomers are available commercially, and they are most commonly elastomers filled with conductive fillers made from silver, copper aluminium, nickel, carbon black or combinations thereof. A drawback of commercially available conducting elastomers is that they are filled to such an extent that adding additional fillers to increase conductivity is not possible. Furthermore, the available conductive elastomers lose their conductivity upon stretching, which is not desirable, since it leads to reduced strains of the elements.

2. Macro-embossing elastomer films

2.1 Introduction

A great obstacle for DEs is stretchable electrodes that have good conductivity and at the same time manage to maintain their conductivity. The way DPP has overcome this issue is by sputtering metal electrodes on corrugated elastomer films, so that when DE is actuated the film expands in area and the electrodes follow the film. Corrugations are essential for the metal electrodes to work, since metals lose conductivity upon stretching. The corrugated elastomer films are prepared by applying a liquid elastomer onto a corrugated carrier web and then curing it directly on the carrier web. The elastomer is then peeled of the carrier web. This step in the process is challenging due to the large surface area, which can cause hundreds of metres to tear in the production process. Therefore, the focus in this study is to investigate how elastomer films can be processed in order to facilitate the use of metal electrodes.

Thermoplastic polymer films are commonly embossed with microstructures by using hot embossing technology. Microstructuring of elastomers is desirable for many products, and so the aim of this study is to investigate the possibility of using technology normally applied to thermoplastics for elastomers, by macro-embossing elastomer films based on knowledge of the mechanical properties obtained from curing profiles.

2.2 Results and discussion

To ease sample fabrication, premixes are prepared whereby one premix contains half the amount of PDMS mixed with the whole amount of crosslinker, a second premix contains the second half of the PDMS with all of the catalyst and a third premix consists of silica nanoparticles mixed with PDMS. This method ensures that sufficient mixing without any reaction can be obtained. First, when the premixes have been mixed, the reaction will start [90].

A curing profile is used to measure over time the storage modulus (G') and the loss modulus (G"), which in this case is, while the sample is curing. For a stoichiometric balanced (r=1) sample, the point where G' and G" are equal to each other is called the "gel point," i.e. the point where a three-dimensional network is formed. For the stoichiometric imbalanced sample the gel point is not the cross point (the point where G' is equal to G")

of G' and G", and so it can be found before the cross point for r > 1 and after for r < 1 [91–94]. However, in this study the cross point has been used as the gel point and as a reference for making the macrostructure well knowing that the cross point is not the exact gel point but from a material property perspective the cross-over is the relevant point.

Curing profiles are recorded for different r-values. Figure 9 shows the curing profiles for r=1.2, r=1.0 and r=0.8, respectively.

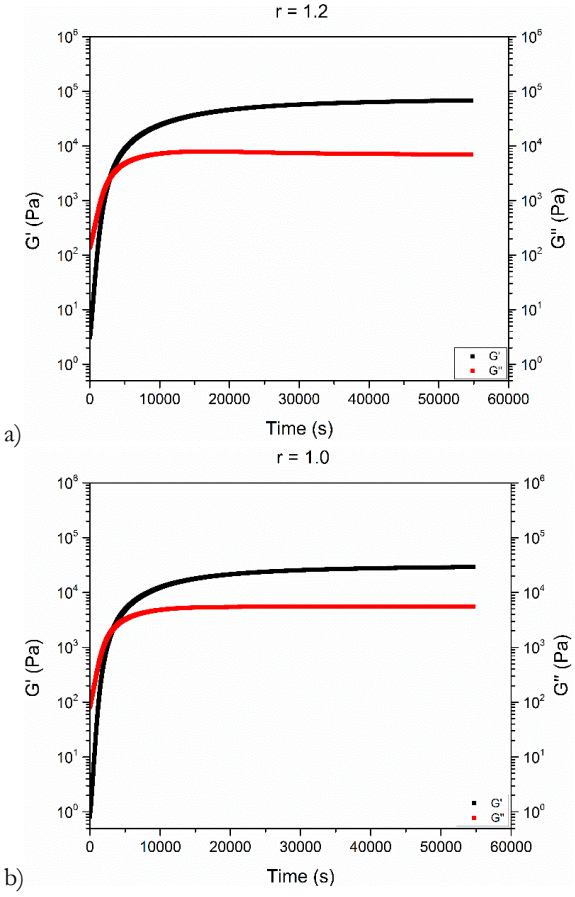

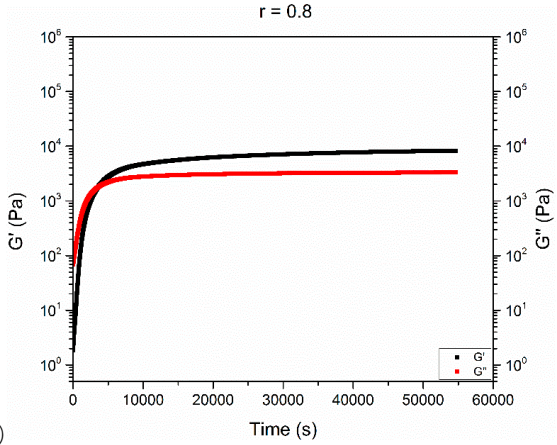

c)

Figure 9 Curing profiles at room temperature for a) r=1.2; b) r=1.0 and c) r=0.8. The gel point is determined to be 69, 65 and 61 minutes, respectively.

The gel point at room temperature for the r-value equal to 0.8 is 61 minutes, for r = 1.0 65 minutes and 69 minutes for r=1.2. This increase is the result of decreased viscosity as well as reduced crosslinker hindrance.

Thickness is investigated for samples with r-values equal to 1.2. The investigated thicknesses are 1 mm and 0.5 mm, which shows that it is possible to emboss a 1 mm film, but as can be seen in Figure 10 the structure embossed 25 minutes after the gel point shows only a sporadic and partial structure in the film.

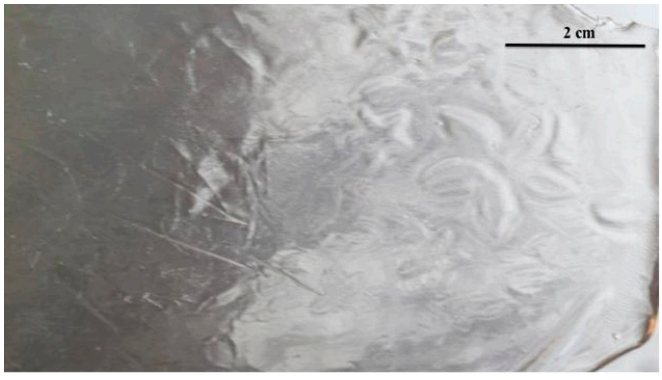

Figure 10 Sample with an r-value of 1.2 and film thickness of 1 mm embossed 25 minutes after the gel point.

Since the structure is not continuous, film thickness is decreased to 0.5 mm and the embossing is performed at the gel point, which is shown in Figure 11.

Figure 11 Sample with an r-value of 1.2 and film thickness of 1 mm embossed at the gel point.

The embossing in Figure 11 is continuous and the indentations and structures are clearer. To determine the possibility of embossing before the gel point, a sample is embossed 30 minutes before the gel point, as depicted in Figure 12.

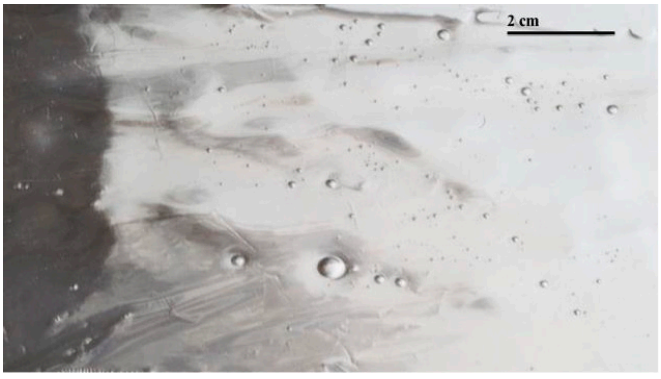

Figure 12 Sample r=1.2. Embossing 30 minutes before the gel point. Only wavy patterns can be observed after final curing.

There are no structures or indentations on the film, which indicates that viscosity is too low and the liquid elastomer has flowed back to its original state.

From the obtained results, the primary parameters are determined and the embossing will be performed after the gel point and on 0.5 mm-thick films. For the r=1.0 samples, embossing is performed from 0 to 30 minutes after the gel point and depicted in Figure 13.

Figure 13 Sample with r=1.0 embossed at a) 0 minutes b) 15 minutes and c) 30 minutes after the gel point.

Figure 13 illustrates embossing performed at various times after the gel point and shows clear and continuous structures for all embossing times. However, the sharpest and more marked structures are obtained when embossing is performed 15 minutes after the gel point.

For the softest material (r=0.8) embossing is performed at time intervals ranging from 0 minutes to 210 minutes after the gel point. Embossing performed 5, 30 and 210 minutes after the gel point is shown in Figure 14.

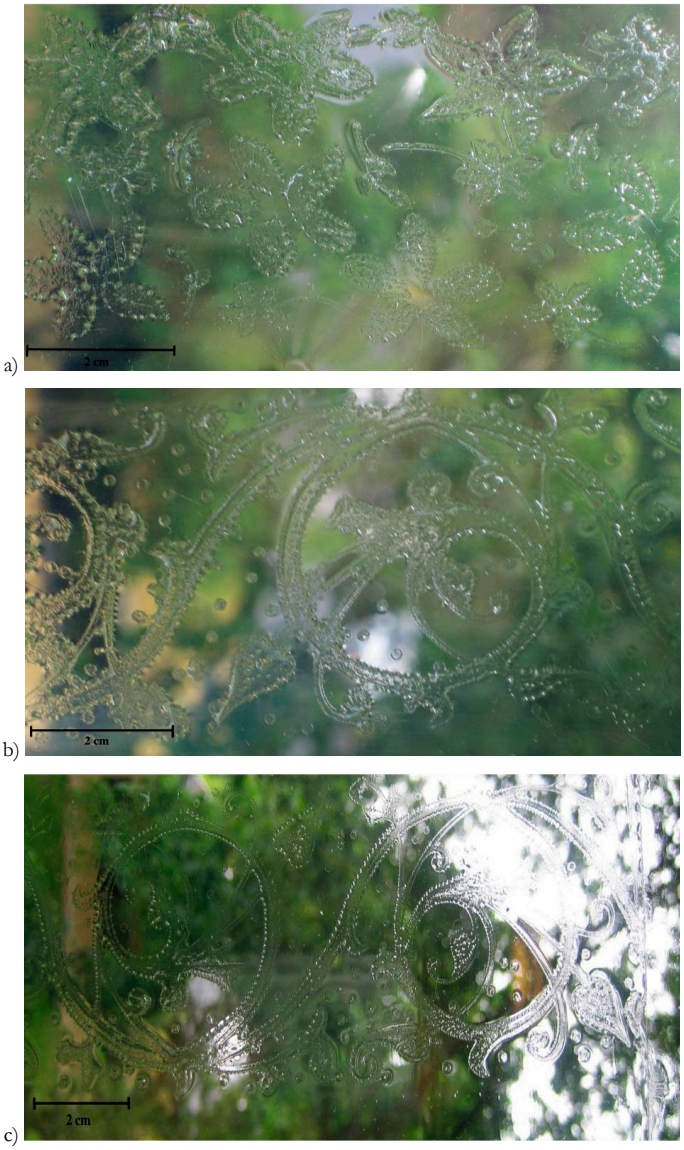

Figure 14 Embossed at a) 5 minutes, b) 30 minutes and c) 210 minutes after the gel point.

The structure in Figure 14A is indistinct, which indicates that embossing should have been performed later. The structure becomes clearer and more distinct when embossing is

performed 30 minutes after the gel point. After 210 minutes embossing is still clear and the indentations are visible.

For all r-values viscosity at the gel point is low, because the samples are to some extent flowing back after the embossing process, so some of the indentations are getting smaller, which can have an effect on the structure when the structure is on the micro scale. If the elastomer film is embossed significantly later than the gel point, the elastomer film will become too elastic and the elastic forces on the film will equal any deformation applied out. A schematic overview of the gel points, time intervals and final elasticities for the r-values is detailed in Table 1.

Table 1 Time interval for macro embossing

r-value	Gel point	Time interval for embossing (after the gel point)	Embossing window	Final elasticity G'(ω ->0) (Pa)
0.8	61 minutes	30-60 minutes	30 minutes	8000
1.0	65 minutes	15-30 minutes	15 minutes	30000
1.2	69 minutes	10-25 minutes	15 minutes	70000

The table shows that embossing is performed later when the r-value is smaller, due to the fact that the film becomes softer as the r-value reduces. This is confirmed by the final elasticities, where G' is highest for r=1.2 and lowest for r=0.8, which indicates that r=1.2 is a harder material than r=1.0, which is again harder than r=0.8. The time interval for r=0.8 is longer than for the other r-values, which is due to the fact that the material is softer and therefore it is possible to emboss for a longer period.

2.3 Conclusion

To minimise or eliminate release issues related to the conventional coating processes for microstructured elastomer films to be used as DEs, a hot embossing method commonly used for thermoplastics was investigated. The study showed that it was possible to emboss macrostructures onto the surface of elastomer films with different stoichiometric imbalances (r=0.8, r=1.0 and r=1.2), using a structured roller. Embossing structures on elastomer film were determined to be performed on films with a thickness set to 0.5 mm. The time interval for embossing is after the gel point, where the embossing is best

performed 10-25 minutes after the gel point for r=1.2, 15-30 minutes for r=1.0 and 30-60 after the gel point for r=0.8.

Based on the obtained results, it was decided that a further investigation of the process was a full-time study, which is beyond the remit of this current work, and so the focus in the present study was therefore decided to be the adhesion of DE films for monolithic elements.

3. Monolithic PDMS laminates for dielectric elastomer transducers via open-air plasma treatment

3.1 Introduction

Multiple DE films are used in the preparation of DE transducers in order to increase the energy density and robustness of a DE element. To eliminate friction between the layers and premature failure, the films are adhered to form monolithic structures which have been prepared by using additional dielectric elastomer as an adhesive, which ultimately increases mechanical resistance. The aim of the work in this chapter is therefore to prepare monolithic PDMS laminates, whereby two PDMS films are adhered in a B2B configuration, without the use of additional dielectric elastomer to adhere the films. This will be achieved by modifying the PDMS surfaces via plasma treatment. The modification of PDMS surfaces enables the adhesion of the films by creating oxygen bonds in the interface.

3.2 Results and discussion

Two approaches to form monolithic structures, both involving plasma treatment, are investigated herein. The first approach involves adding aminosilane bis(3-(trimethoxysilyl)propyl)amine as an adhesion agent between the modified surfaces. In the second approach, the films are plasma-treated and then adhered together.

3.2.1 Aminosilane

Elastosil RT625 films are plasma-treated for two minutes using a conventional plasma treater. After plasma treatment, two drops of the aminosilane are dropped onto the surface and a second film is placed on top with the treated surface downwards. Rheological measurements are performed on a non-treated single film, a plasma-treated laminate and a laminate with aminosilane as an adhesion agent, all of which are depicted in Figure 15.

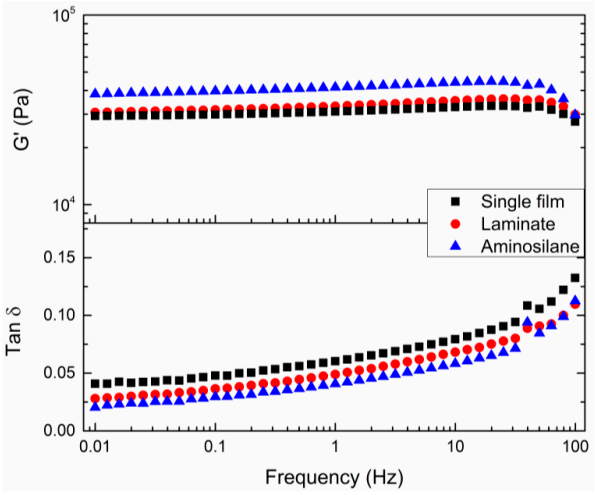

Figure 15 Linear viscoelastic properties of a single film, plasma-treated laminate and aminosilane laminate at 23°C. Thickness of the single film is 0.5 mm and 1 mm for laminate, respectively.

Figure 15 shows that the aminosilane-laminate is slightly stiffer than the single film and the plasma-treated laminate, the latter of which has the same elastic properties as the single film. Furthermore, qualitative analyses on the tear strengths of the laminates are performed and show that aminosilane-laminates are fragile and tear at low stretches. Since plasma-treated laminates show similar elastic properties as single films, and due to the fragility and stiffness of the aminosilane laminates, the focus moves towards using plasma treatment only as a method to enable the adhesion of PDMS surfaces.

3.2.2 Open-air plasma

Conventional plasma treatments are performed in a vacuum, which is highly expensive when used on an industrial scale. To potentially decrease these processing expenses, an open-air plasma treatment system is used for modification, replacing the vacuum-based method.

The focus in this study is to determine optimal parameters necessary to perform the plasma treatment, such as speed and distance to the nozzle, by investigating the mechanical and electrical properties of the monolithic layers, as well as the peel force, to determine if the laminates will detach during operation.

Samples are prepared by plasma treating the surface of LR3043/30 films. The treated films are adhered together on the treated side and laminates are formed. The plasma treatment is

performed at different distances from the sample to the nozzle and at different speeds across the films. For rheological measurements, samples have a diameter of 25 mm, single film a thickness of 0.5 mm, and laminate a thickness of 1 mm. For the dielectric and peel measurements, samples have a thickness of 80 μm.

To determine the influence of the plasma treatment on the surface of the elastomer films, SEM micrographs along with EDS spectra are recorded for both treated and non-treated films, and are shown in supporting information. The obtained SEM micrographs and EDS spectra show no obvious differences, which indicates that the only differences – if any – are on a molecular level.

Mechanical properties

Rheological measurements are performed to investigate the mechanical properties of a laminate and then to determine if the plasma-treated interfacial layer has changed the overall mechanical properties of the film. In particular, it is important to determine if the laminates have higher interfacial stiffness, since stiffness in the interface will cause a reduction in actuation or cause disruption to the interface upon actuation. Mechanical properties of a plasma-treated sample are compared with a single non-plasma-treated film. The storage and loss moduli are depicted as functions of applied frequency at 23°C in Figure 16.

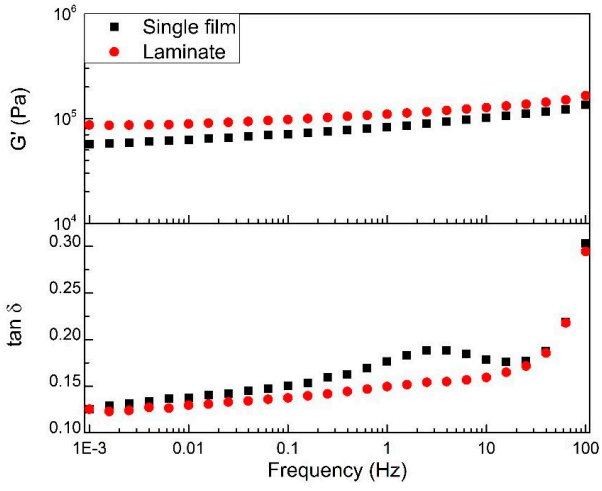

Figure 16 Linear rheological data of a laminate compared to a single film of LR3043/30 at 23 °C. Thickness of single film is 0.5 mm and 1 mm for laminate, respectively.

The storage modulus (G') shows a minor increase for the laminate compared to the single film. This minor difference can be ascribed to the difference in thicknesses of the samples, and it is not expected to be the result of a stronger interfacial bond. At low frequencies, the loss tangent, tan δ, is comparable with the single film, whereas at frequencies between the 1 and 10 Hz the laminate has a lower loss than the single film. This can be explained by a reduction of surface area per volume[95], which confirms the monolithic nature of the laminate.

Electrical breakdown strength

Electrical breakdown strength is measured for the laminate at the previously specified distances and speeds, to investigate if plasma treatment influences breakdown strength. Furthermore, the measurements are performed on single films, where both plasma-treated and non-plasma-treated films are investigated. Breakdown strengths for the different samples are shown in Figure 17.

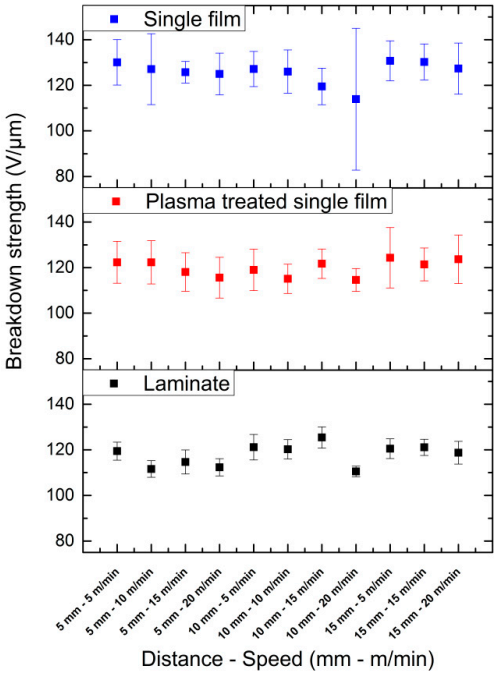

Figure 17 Breakdown strength for LR3043/30 laminates, where plasma treatment is performed at different distances to the nozzle and speeds. Single films have a thickness of 40 µm and laminates a thickness of 80 µm. The breakdown strengths illustrated are averages of 12 measurements.

Figure 17 shows that breakdown strength decreases after plasma treatment for both single films and laminates for all distances and speeds. There are no obvious correlations between the decrease in breakdown strength and the distances and speeds at which the samples are treated. A moderate decrease in breakdown strength is observed for the plasma-treated single films compared to the non-treated single films, which is due to the formation of polar silanol groups on the surface during plasma treatment. For the laminates, the decrease in breakdown strength is due to higher sample volume and thus the higher likelihood of encountering a defect in the test specimen. Furthermore, during breakdown measurement, when high voltage is applied across the film volumetric Joule heating is expected[11]. For thicker films the removal of the excessive heat is slower than for thinner films, which subsequently will decrease breakdown strength as conductivity increases in line with increased temperature[96]. Zakaria et al.[96] measured breakdown strength for samples as single films with various thicknesses as well as samples consisting of multiple layers. The breakdown strength for 40-80 μm-thick liquid silicone rubber is shown to decrease significantly in line with increasing thicknesses. Zakaria et al.[96] showed that breakdown strengths of thicker single films decreased by 43% compared to thin films and the multiple layer samples decreased by 31%. In comparison, the plasma-treated films in this study decreased by only 6% in breakdown strength, which shows that the plasma treatment of the interface conserves breakdown strength and provides a more homogeneous laminate, which in turn confirms the monolithic structure of the sample.

Peel forces

The interfacial layer strength is additionally investigated through a study of peel strength, as shown in Figure 18.

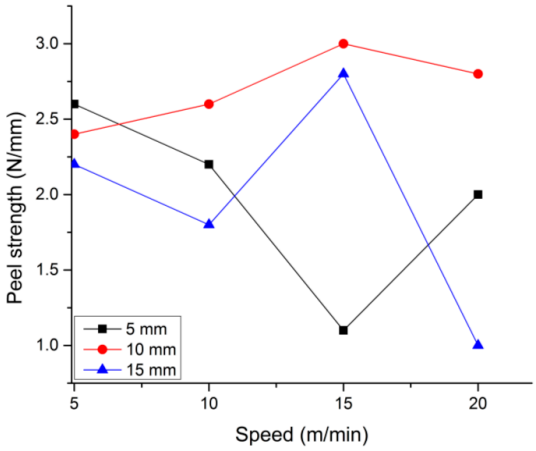

Figure 18 Peel forces of LR3043/30 laminates at room temperature.

Peel strengths for the samples performed at distances of 5 and 15 mm are generally lower than what is observed at a distance of 10 mm to the nozzle. In addition, a much higher scattering of data is observed at these distances, with varying application speeds. An explanation for the observed variation could be that the dosage is either too high or too low to provide a uniform treatment of the sample, and if the distance is too short, the intensity of the plasma might be too high and will therefore result in a more severe change of the surface energy of the film, which will result in poorer interfacial adhesion. If the distance is too high, though, this will lead to the intensity of the treatment being too low and the surface will not be significantly modified, thereby resulting in an insignificant reaction on the interface. Plasma treatments performed at a distance of 10 mm show small variations in the peel forces at different application speeds and generally provide the strongest interface. Both the variation and the strength of the interface indicate that this is the optimal distance away from the sample to the plasma nozzle, where a sufficient degree of modification of the film surfaces has taken place, thus ensuring good interfacial bonding.

3.3 Conclusion

To improve the performance of DE transducers multiple layers need to be adhered together to form monolithic structures. The study shows that it is possible to adhere PDMS surfaces in a B2B configuration using both approaches; however, using aminosilane as adhesion agent, the laminate increases in stiffness and the tear strength decreases. By eliminating the use of

additional dielectric material as well as an adhesion agent, the laminates are prepared by only plasma-treating the surfaces and adhering the films. The obtained results show that open-air plasma treatment is a suitable method for pre-treating PDMS films before adhesion and that it results in high-strength laminates performing as monolithic elements, without increasing the thickness of an element.

4. Design of an elastomer structure to facilitate the incorporation of expanded graphite in silicones, without compromising electromechanical integrity

The work in this chapter is based on the published paper *Design of elastomer structure to facilitate incorporation of expanded graphite in silicones without compromising electromechanical integrity* published in *Macromolecular Materials and Engineering*, 2015, **300** (5), pp. 542-550 and reprinted with the kind permission of Wiley. The manuscript can be found in Appendix B.

4.1 Introduction

The aim of the study in this chapter is to prepare adhesives for F2B and F2F configurations.

The filler, EG, has great conductive properties and has the advantage of not increasing the stiffness of the composite substantially. At a loading of 5 wt% the percolation threshold is reached and the composite becomes conductive. However, at loadings above the percolation threshold, network destruction was observed [97], and for this reason it is interesting to investigate the use of EG fillers in preparing high dielectric permittivity materials.

Therefore, in this study, EG is dispersed in a reinforced PDMS matrix to increase the dielectric permittivity of the composite and eventually to increase EG concentration to produce conductive elastomers. The PDMS matrix is reinforced by using an 8-functional crosslinker, and the elastomer network is loaded with various concentrations of EG (2-4 wt%) to investigate the electromechanical properties of more compliant networks with less voids – and thus better electromechanical properties.

4.2 Results and discussion

Natural graphite consists of multiple sheets of graphene held together by Van der Waals forces, as shown in Figure 19a. By introducing the graphite to small molecules, e.g. acids[98,99], between the graphene layers, followed by rapid heating, the Van der Waals bonds are broken, the acid is vaporised and the graphene sheets separate (Figure 19b). This

type of graphite can be dispersed into the polymer matrix and provides an exfoliated graphite composite, as illustrated in Figure 19c.

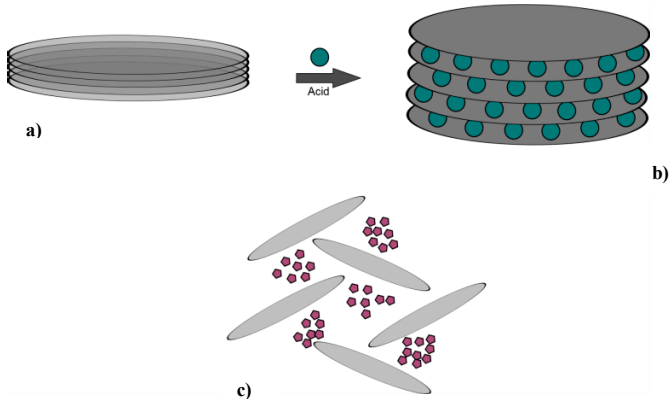

Figure 19 Different types of graphite a) natural graphite, b) expanded graphite and c) exfoliated graphite.

PDMS samples were prepared with different concentrations of expanded graphite by speed mixing them to obtain well-dispersed samples. To ensure a good mixing of the catalyst and crosslinker into the PDMS precursor, premixes were prepared, thereby simplifying the process as well as allowing for the storage of premixes.[90] It was previously shown that speed mixing is an efficient way to disperse EG in silicones.[97]

4.2.1 Morphological analysis

The morphologies of cured 1 wt% EG-loaded samples from mechanically mixing and speed mixing, respectively, are shown in Figure 20.

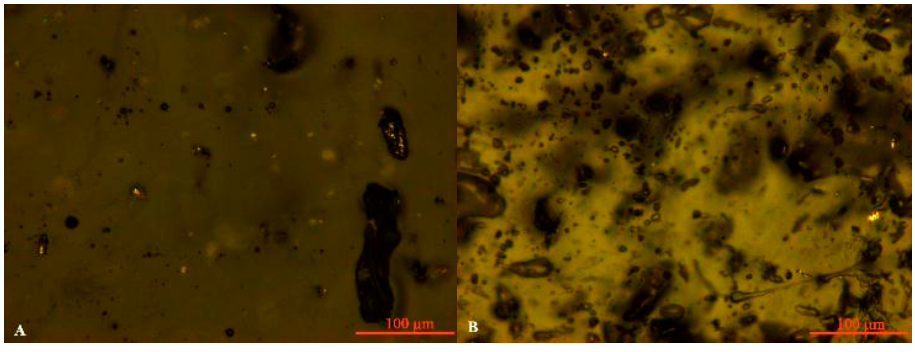

Figure 20 Optical microscopic images of the dispersion of EG in a mechanically mixed sample (A) and a speed-mixed sample (B) with a concentration of 1 wt%.

The mechanically mixed elastomer contains big EG filler agglomerates, and so we can conclude that the mechanical mixing is not sufficient to break the agglomerates and thereby achieve the good micro-scale dispersion of the fillers in the PDMS matrix. By speed mixing the sample the agglomerates are broken down to a larger extent and the EG fillers are better dispersed throughout the sample, as illustrated in Figure 20B. Particle size varies widely for the mechanically mixed samples, from agglomerates of lengths ~200 μm, which are rather common, to the speed-mixed samples where the largest agglomerates are of the order of 50 μm.

4.2.2 Mechanical properties

A small amplitude oscillatory shear is used to investigate mechanical properties and to establish how the fillers influence the network. The linear viscoelastic properties for the samples with different loadings and a reference sample (Elastosil RT625) are compared and illustrated in Figure 21.

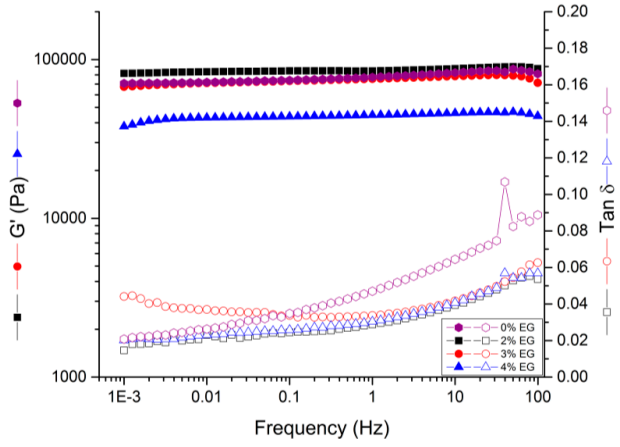

Figure 21 Linear viscoelastic properties of the PDMS-V35 network with different EG loadings compared to the unfilled benchmark elastomer Elastosil RT625.

Figure 21 shows that the storage moduli decrease in line with the increased loading of the EG fillers. The storage moduli for the 2 and 3% loaded samples are comparable with the benchmark silicone elastomer Elastosil RT625 within +/-10%, which is within common uncertainty in relation to the determination of G´ for soft elastomers. The sample with a concentration of 4% has a significantly lower storage modulus (~ a factor of 2), which is not what is commonly encountered in composites of thermoplastic polymers which usually

show increases in G' in line with loading. Seen from the perspective of the actuation equation (Eq.1), the decreased storage modulus is favourable, since $Y=3G'(\omega \rightarrow 0)$ and thus increased actuation should be obtained solely from the decrease in G'. However, this behaviour indicates that major network destruction is taking place.

The increased interfacial area with increased loading could impose steric hindrance and a reduction of mobility in the matrix, which is well-known for nano-composites. This in turn would result in a slower or incomplete reaction and especially affect systems with an already reduced volume, as in a thin film system. In a similar manner, the increased surface area of the filler in the well-dispersed reaction media could interact with the platinum catalyst and inhibit the reaction, which again would result in a slower or incomplete reaction. The observed reduction in moduli through the improved dispersion of the filler could also be explained based on steric hindrance around the particles, which would result in local internal two-dimensional (2D) curing, which is in contrast to traditional 3D curing of the elastomer in the bulk. On the surface, the dynamics of the crosslinker are reduced significantly, since the crosslinker relies on self-diffusion rather than on reptation[100]. Furthermore, the number of reactive sites surrounding the interface crosslinker is reduced by a factor of approximately two, and thus the crosslinker becomes more susceptible to participating in loop formations or simply not reacting. Both phenomena lead ultimately to the crosslinker becoming a chain extender and thus decreasing effective crosslinking concentration. For the 4-functional crosslinker the formation of one loop causes the loss of crosslinking capability, while two unreacted sites have the same effect. For the 8-functional crosslinker, three times as many occurrences are required.

This surface phenomenon is observed very often at the macroscopic level for Pt-catalysed silylation room temperature vulcanised silicone (RTV), where the surface of a sample may feel sticky or greasy, whereas the bulk is completely non-sticky and fully cured. If this phenomenon is taking place, it would be expected that increased dispersion of the filler would result in a reduction in the storage moduli of the samples and the formation of small voids in the system.

In a previous study a 4-functional crosslinker was used[97]. Upon comparison of the 8-functional system with the previously studied 4-functional crosslinked system, it is evident that the storage moduli are lower for the 8-functional crosslinked system with the 3% and 4% EG-loaded samples and higher for the 2% EG-loaded sample. This behaviour can be explained as being the result of the better incorporation of the 3% and 4% EG in the 8-

functional network compared to the 4-functional network. For the 2% loaded samples, dispersion is good in both types of networks, and the 8-functional network thus has the highest elastic modulus – as predicted by classical network theories.

Table 2 shows the storage and loss moduli at 0.01 Hz and the viscous loss of each network.

Table 2 Mechanical properties at room temperature and at 0.01 Hz.

Sample	G' [kPa]	G" [kPa]	Tan δ
2% EG	84	1.9	0.023
3% EG	71	2.6	0.037
4% EG	43	1	0.023
RT625	72	1.9	0.026

The greatest viscous loss can be seen for the 3% EG-loaded sample, while the 2 and 4% examples have viscous losses similar to that of Elastosil RT625. This behaviour can be explained by the higher tendency to employ 2D curing, which thus decreases G' when loading.

In an earlier study[97], a 4-functional crosslinker was used to crosslink the matrix. The study showed that relative viscous dissipation between 100 and 0.01 Hz was of the order of ten times higher than what is reported herein. This is the result of 2D curing and the occurrence of voids in the matrix. By using an 8-functional crosslinker this phenomenon is eliminated and the matrix improves significantly.

4.2.3 Dielectric properties

Dielectric permittivity is measured for all DMS-V35 samples loaded with EG (2-4 wt%) and the pure Elastosil RT625 on the ARES G2 with a dielectric thermal analysis fixture. Figure 22 illustrates dielectric measurements for the EG-loaded samples with different loadings of EG and RT625 (0 wt% EG).

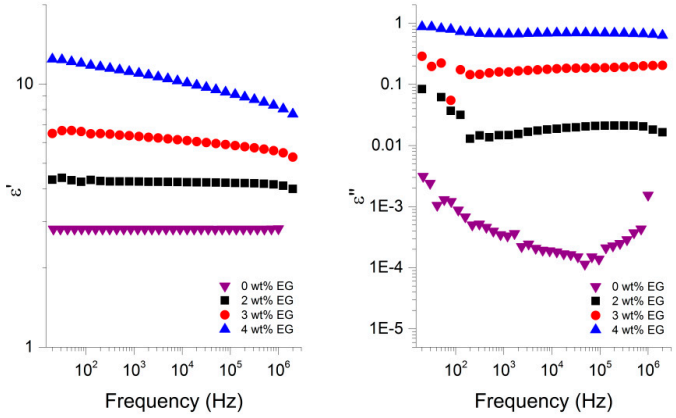

Figure 22 Dielectric permittivity measurements for the different loadings of EG and Elastosil RT 625 at room temperature.

The results show that by increasing the loading of EG, permittivity increases as expected. The permittivity for the 2 and 3 wt% loaded samples and RT625 are almost constant over the whole frequency range while the permittivity for the 4 wt% loaded sample is decreasing with increasing frequency, showing a strong tendency to Maxwell polarization at low frequencies.

In a previous study[97], where the PDMS matrix was vulcanised with a 4-functional crosslinker, permittivity was measured at 8.6 for the 4% EG-loaded sample. This increase in permittivity was caused as a result of the large surface area of the particles being active. For the 8-functional crosslinked system, dielectric permittivity was measured at 12, which is a 40% increase over the 4-functional crosslinked system and a 375% increase in relation to the commercially available Elastosil RT625 system. This increase in dielectric permittivity could be caused by the improved matrix facilitating better distribution, while crosslinking density would also determine mobility in the network.

Electrical breakdown strengths, which were measured for the different loadings and compared to the benchmark silicone elastomer, are depicted in Figure 23. The error bars for each sample measurement are shown as vertical lines and indicates the deviation of the 12 measurements performed for each sample.

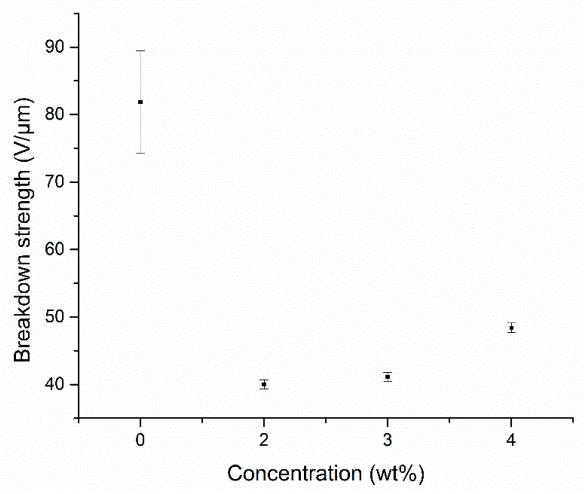

Figure 23 Breakdown strength of the various composites at room temperature

The figure shows an increase in breakdown strength in line with increasing EG loadings. Breakdown strengths are 40 V/μm, 41V/μm and 48 V/μm for the 2% EG, 3% EG and 4% EG-loaded samples, respectively. However, in comparison with the benchmark, breakdown strength (81 V/μm) decreases by a factor two, due to a combination of increased conductivity, changed morphologies (the benchmark material contains non-conductive silica fillers which reinforce the material) and mechanical properties when EG is added to the otherwise homogeneous silicone elastomer.

The standard deviation on the reference film is +/- 7 V/μm, which is rather large but not uncommon when several breakdown phenomena are occurring simultaneously [101]. For those elastomers with EG, standard deviations drop to +/- 2 V/μm, which indicates that there is one single phenomenon causing electrical breakdown. Samples with un-optimised network showed strong dependence on the location of the electrode when testing for breakdown strength, such that variations in determining breakdown strength were very large, with data scattered in between 20 and 50 V/μm, thereby indicating the very non-homogeneous distribution of EG. These samples were therefore not suitable candidates for dielectric elastomers, as they would fail instantaneously when the entire elastomer, rather than just single points, was subjected to an electrical field.

4.2.4 Electromechanical properties

The actuation performance of the materials with different EG loadings was measured on 120-150 μm thick films. These thicknesses were chosen in order to exceed the largest particle sizes and thus avoid single-particle short-circuiting. Different voltages (1-5kV) were applied to 10% pre-stretched samples and the subsequent force was measured. The pre-stretch method was introduced to soften the elastomer slightly as well as to avoid uncertainty regarding the zero-stress state of the elastomer and thus reduce measurement uncertainties due to wrinkling etc.

The electrical field as a function of the strain is illustrated in Figure 24. The figure shows, as expected, that the strain increases slightly faster for 3% EG in line with increasing the electrical field. For the 2% sample there is good agreement between the results from the electrical breakdown measurements (Figure 23), whereas for the 3% sample coupled electromechanical breakdown strength reduces by approximately 8 V/μm, which indicates that electrical breakdown strength decreases in line with EG plate alignment.

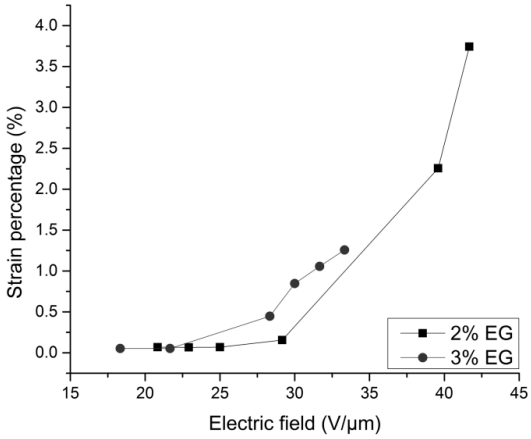

Figure 24 Sample actuation curves for the 2% and 3% EG loadings.

Measured actuation performance is compared with predicted actuation, which is illustrated in Figure 25. Predicted actuation performance is calculated from measured dielectric permittivity and the Young's modulus using Eq. 1. Figure 25 shows that the actual measured strains are not consistent with the predicted measurements, which can be attributed to heating arising from both electrical and mechanical losses, thereby leading to an increased leakage current before the electrical field becomes so large that it exceeds any

leakage. A recent study by Zakaria et al. [11] showed that even changes of as little as 10°C can potentially lead to detrimental dielectric elastomer behaviour. Furthermore, air voids may be introduced upon stretching, thus leading to lower actuation.

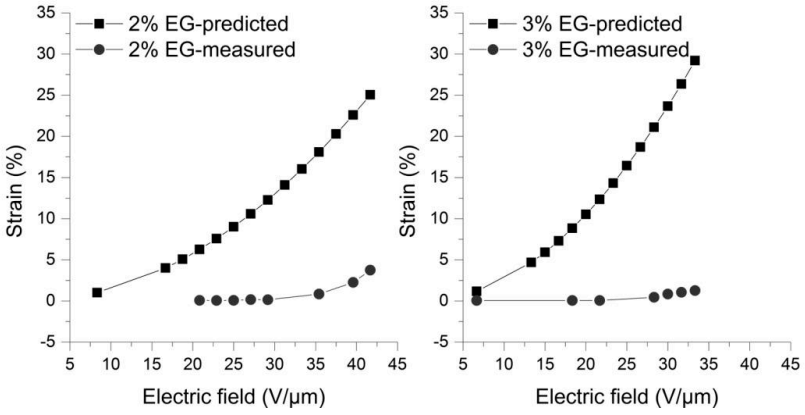

Figure 25 Experimental versus theoretical actuation of the composites at room temperature.

The differences between predicted and measured actuation at higher electrical field are approximately a factor of five for the 2% EG-loaded samples and approximately 30 for the 3% EG-loaded sample. Differences in the measured and predicted values could have been caused by a leakage current, which indicates that the material is not a perfect insulator and has some conductivity. Breakdown may also be facilitated by voids at the interfaces upon stretching, where local deformation may be anisotropic due to weak interfacial forces between EG sheets and the silicone matrix.

The dimensions of the EG sheets are of the order of 60 μm (as determined from the optical images in Figure 20B). For comparison, the end-to-end distance of the polymer applied in this study is calculated[102], and it is assumed that the PDMS polymer chain has an average molecular weight of $\overline{M}_n$=50 kg/mol, the average bond length is 1.5 Å and that the polymer chain can be described by a simple random walk with the step length of the repeat unit [-Si$(CH_3)_2$-O-] (M_o=74 g/mol). The number of repeat units is $N=\overline{M}_n/M_o$=50103/74=677, and the length of one repeat unit consisting of two bonds is b=2*1.5Å=3Å. The (random walk) end-to-end distance is $R=\sqrt{N}*b=\sqrt{677}*3Å=78Å$, while the area of an EG plate is assumed to be 60 μm*60 μm. From these calculations it is obvious that the 2D effect is rather significant, since the area of one EG facilitates

approximately $6*10^7$ 2D crosslinks. This large number indicates the significance of the local environment of the interface between the elastomer and EG. Therefore, it is important that the crosslinker provides the possibility of forming a 2D network on the surface with similar stress-releasing properties as the matrix, such that stress-induced voids are minimised. The 8-functional crosslinker facilitates a stronger network on the surface, since it does not need to react fully in order to act as a crosslinker, whereas the 4-functional crosslinker acts as a chain extender if two of the reactive sites react with the same end-functionalised PDMS, i.e. a loop, or if the local environment allows for two reactions only.

4.3 Conclusion

As mentioned in Chapter 1, fillers are added to PDMS in order to improve dielectric permittivity, and Eq. 1 is used as the basis for optimising DEs.

This study shows that using EG as a filler in PDMS networks increases dielectric permittivity significantly compared to a reference sample. However, dielectric loss also increases, which means that a larger amount of energy is dissipated as heat. This can be seen in the actuation measurements, where the measured actuation is approximately five times lower than the predicted measurements for 2% EG and approximately a factor of 30 for the 3% EG. Furthermore, the mechanical properties were investigated and showed that the material became softer in line with increasing EG loadings. This is explained by the two-dimensional curing taking place at the interface between the silicone and EG. Electrical breakdown strength increases in line with increasing EG loadings, where the breakdown strength is 40 V/μm for the 2% EG, 41 V/μm for the 3% EG and 48 V/μm for the 4% EG sample. Compared to the benchmark, breakdown strength decreases by a factor two, though this was expected, since the benchmark is filled with non-conductive silica particles.

The obtained results indicate that even by improving the matrix by using an 8-functional crosslinker, EG influences the overall performance of material even at low EG concentrations in the matrix. Increasing the concentration further, to make conductive elastomers, will increase dielectric losses and the material will become softer due to two-dimensional curing.

5. Dispersing carbon nanotubes in PDMS and its influence on electrical and mechanical properties

5.1 Introduction

This chapter focuses on the preparation of conductive elastomers that can be used as adhesive for electrical connection as well as for both the F2B and F2F configurations. In Chapter 4, EG was used as a filler, and network destruction was observed even at concentrations below the percolation threshold. Therefore, CNTs are used as fillers, since the particle size is smaller and the percolation threshold is significatly lower than for EG fillers, while in addition lower loading is needed in order to prepare conductive composites. Furthermore, the prepared conductive elastomers are not to be used as electrodes, and due to the DE film corrugations the stretchability of the conductive elastomer is not of great importance.

The dispersion of CNTs is challenging, so two approaches to disperse CNTs into the elastomer matrix have been investigated. The first approach involves adding IL as a dispersion agent, whereby the CNTs are ground with an IL, and the second invovles a covalent modification where functionality is grafted to the CNTs. Two dispersion methods are investigated, in which IL is added as a dispersion agent.

The first dispersion method requires one to ultrasonicate the CNTs in the presence of a solvent and then add the CNTs to the PDMS. The second dispersion method uses a roll mill to disperse the CNTs in the PDMS. Furthermore, the influence of IL on dispersion, and ultimately electrical and mechanical properties, is investigated.

5.2 Results and discussion

The dispersion of CNTs in an elastomer matrix, in order to increase conductivity for the preparation of conductive elastomers, is investigated. Elastosil RT 625 is used as the polymer matrix due to its great adhesion properties. Multi-walled CNTs (MWCNTs) and 1-ethyl-3-methyl imidazolium bis (triflouromethanesulfonyl)imide are used as CNTs and IL, respectively. In the first section, two dispersion methods are investigated for CNTs dispersed in a PDMS matrix, and IL is used as a dispersion agent. In the second section the results for functionalised CNTs dispersed in a PDMS matrix are discussed.

5.2.1 Carbon nanotubes dispersed with ionic liquids

ILs have been shown to ease the dispersion of CNTs, and they are used in this study to investigate their effect on dispersion. Firstly, the CNTs are dispersed by ultrasonication, where CNT and IL concentrations are investigated. Secondly, the CNTs are dispersed by roll milling, while samples prepared with IL as a dispersion agent are compared to samples without IL.

Dispersion of CNTs by ultrasonication

Samples are prepared by grinding CNTs with IL until gelation occurs. Solvent is added to the CNT/IL mixture and the solution is ultrasonicated. After ultrasonication, part A of the polymer matrix is mixed with the CNT/IL mixture. The solvent is then evaporated and part B is added and mixed to make the CNT/IL/PDMS composite. A detailed description of the sample preparation can be found in Chapter 7. Concentrations, ranging from 1 wt% to 5 wt%, are prepared and the CNTs are dispersed with IL in a 1:1 weight ratio. The conductivities of the resulting samples are shown in Figure 26.

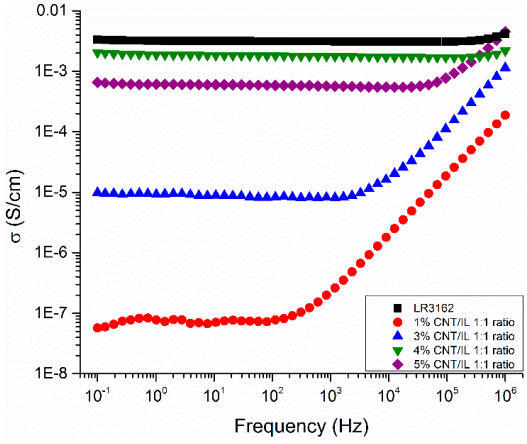

Figure 26 Conductivity measurements for CNT/IL/PDMS composites with different CNT concentrations. CNTs and IL are mixed in a 1:1 weight ratio.

Initially, conductivity is seen to increase in line with increasing concentrations of CNTs, as expected. However, concentrations above 4 wt% cause a reduction in the accessible surface area, and conductivity suddenly drops. This indicates that the CNT/IL fillers form

agglomerates and the limit for loading CNT/IL into the matrix has been reached. Furthermore, it can be seen that frequency dependency decreases in line with increasing CNT concentrations, which could suggest a better dispersion of CNTs in the matrix, due to higher shear forces[103]. Figure 27 depicts the linear viscoelastic properties of samples, with concentrations ranging from 1 wt% to 5 wt%, and with a 1:1 CNT:IL ratio.

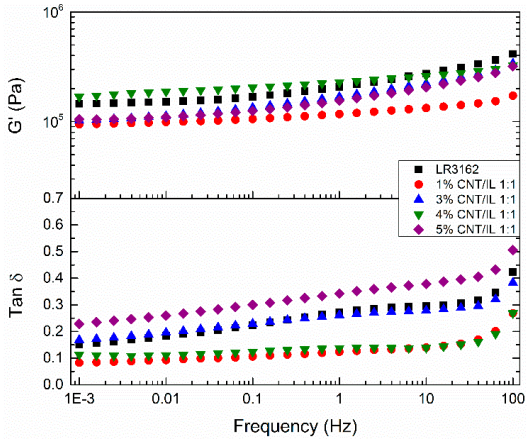

Figure 27 Linear viscoelastic properties of CNT/IL/PDMS composites with different CNT concentrations.

The composites become stiffer in line with increasing concentrations of CNTs; however, for the sample containing 5 wt% CNTs, G' decreases, which indicates that the network is being destroyed, as explained in Chapter 4. The decrease in G' can also be explained as the reduction of mobility due to the increased interfacial area. This confirms that the limit for loading CNT/IL to the matrix has been reached. Tan δ increases in line with increasing concentrations of CNTs. The composite with 4 wt% CNTs shows losses lower than the composite with 3 wt%, thereby confirming good CNT dispersion.

The influence of IL on conductivity is investigated, and the conductivities of samples containing 1 wt% CNT with different ratios of IL are shown in Figure 28.

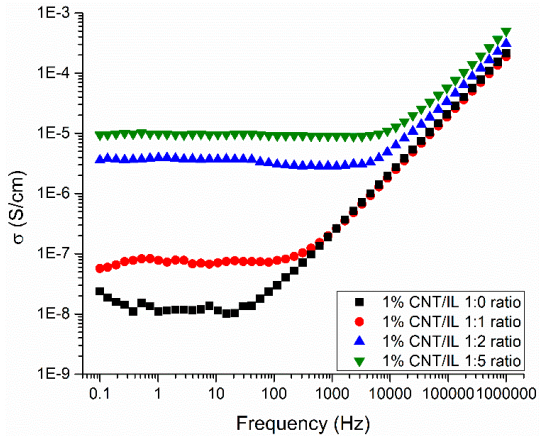

Figure 28 Conductivities of 1 wt% CNT samples with different ratios of IL.

Conductivity increases in line with increasing amounts of IL. The greatest impact is seen with the 1:1 and 1:2 weight ratios, where conductivity increases dramatically. This could indicate that the CNTs have broken away from the clusters and are well-separated into single tubes within the matrix; additionally, increasing IL concentration further will not influence conductivity substantially. Frequency independency at higher frequencies confirms better dispersion associated with increasing concentrations of IL. Linear viscoelastic measurements of 1 wt% samples with various IL concentrations are shown in Figure 29.

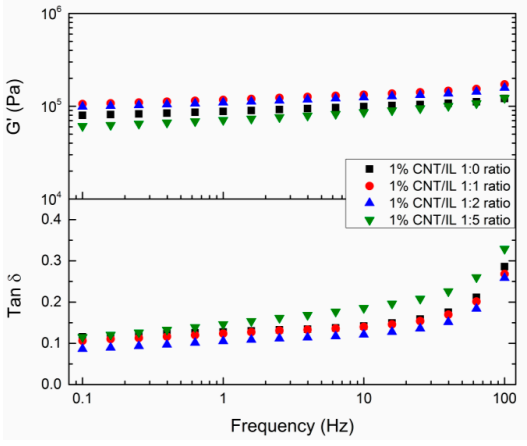

Figure 29 Linear viscoelastic measurements of 1 wt% CNT samples with different ratios of IL.

The results show that increasing the IL concentration to a 1:5 ratio softens the composite slightly and the loss tangent (Tan δ) increases. This indicates network destruction at high concentrations of IL.

In Figure 26, it is evident that the highest conductivity with a 1:1 weight ratio is obtained with a concentration of 4 wt%, and due to network destruction at the 1:5 CNT:IL weight ratio, IL concentration increases to a 1:2 ratio for a 4 wt% CNT composite, the resulting conductivity of which is depicted in Figure 30.

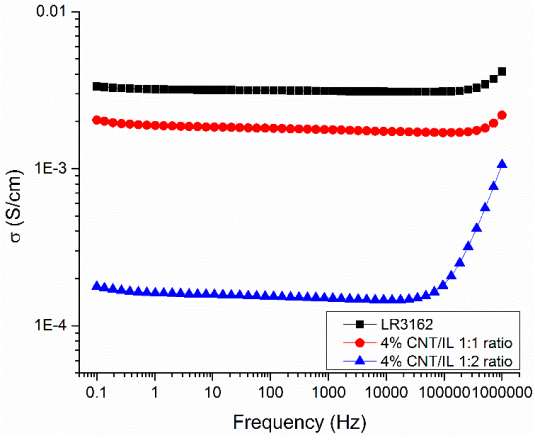

Figure 30 Conductivities of 4 wt% CNT samples with different ratios of IL.

However, conductivity decreases in line with increasing IL-concentration for samples loaded with 4 wt% CNT. A second samples with 4 wt% and 1:2 CNT:IL ratio is prepared and showed a further decrease in the conductivity. Therefore the 4 wt% sample with a 1:1 CNT:IL ratio is tried reproduced and the measured conductivities are depicted in Figure 31.

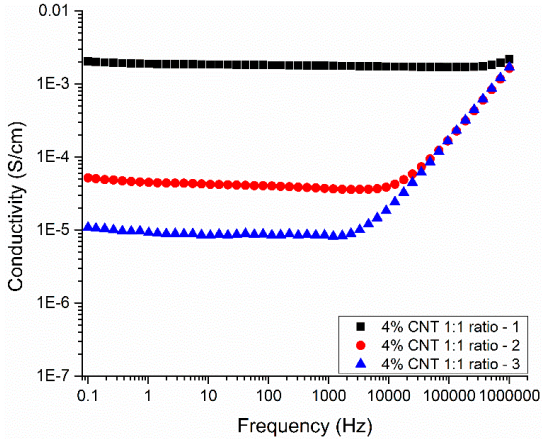

Figure 31 Reproduction of 4 wt% CNT samples with a 1:1 CNT:IL ratio on a glass-glass substrate.

The figure shows that conductivities are not reproducible. This may be due to the many steps in the preparation process that can influence the final sample. One step in particular that can have a major influence is the grinding of the CNTs with the ILs, since this is done manually.

Furthermore, the substrates on which the samples are cast are also investigated to determine if the substrate influences conductivity, as illustrated in Figure 32.

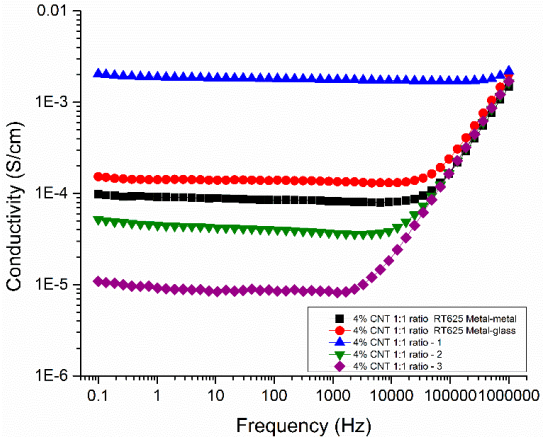

Figure 32 Reproduction of 4 wt% CNT samples with a 1:1 CNT:IL ratio on different substrates.

The deviation in conductivities for different substrates, as well as on the same substrate, shows that the substrates do not influence conductivity. If the CNTs are not ground

adequately, the CNTs agglomerate, which leads to a smaller surface and subsequently lower conductivity. Therefore, in order to increase the CNT surface in the polymer matrix, roll milling as a dispersion method is investigated.

Dispersion of CNTs by roll milling

Samples are prepared with concentrations of 4 and 5 wt% CNT, and the samples are then dispersed with IL in a 1:1 ratio and compared with samples without IL. These concentrations are chosen particularly since they showed the highest conductivities and to investigate if the dispersion can be improved in order to increase the conductivity further. The conductivities of the roll milled samples are shown in Figure 33.

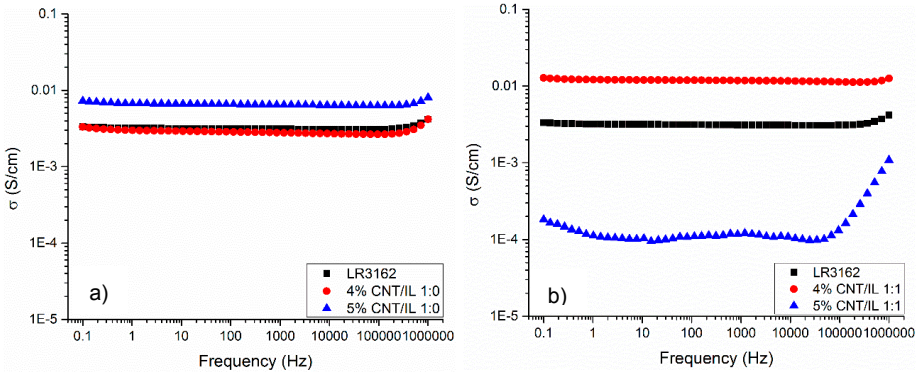

Figure 33 Conductivity measurements at room temperature for samples dispersed using a roll mill, a) without adding ILs and b) with IL in a 1:1 ratio.

For samples without IL, conductivity increases in line with increasing concentrations of CNTs, while it decreases in line with an increase in CNT concentration for the samples dispersed in IL. This tendency can be seen in both dispersion methods and shows that IL influences conductivity negatively when the CNT concentration increases.

Rheological measurements are performed and depicted in Figure 34.

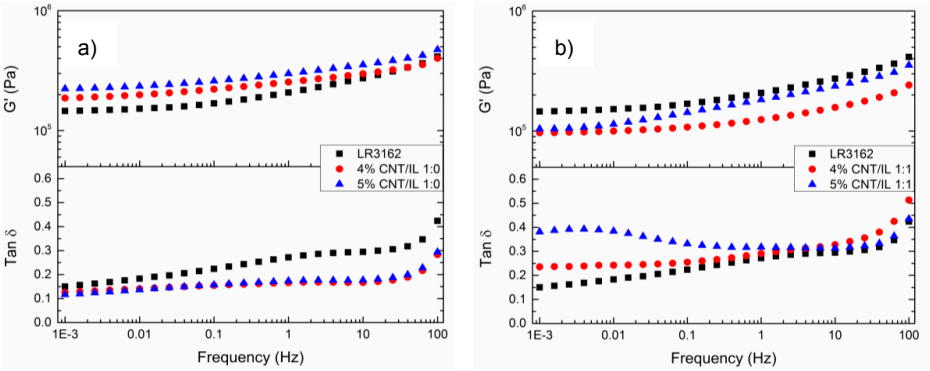

Figure 34 Conductivity measurements for samples dispersed using roll mill with IL in 1:1 ratio at room temperature.

For the samples without ILs, G' increases in line with increasing concentration of CNTs and the samples are stiffer that the commercially available Elastosil LR3162. However, when the CNTs are dispersed with ILs the composites get softer. The conductivity of a composite is influenced by the dispersion of a given filler in a polymer matrix, whereby the better the dispersion, the higher the conductivity. Furthermore, mechanical properties are influenced by the addition of fillers in the matrix. Above the percolation threshold, these fillers are capable of forming a particle network which will significantly increase G'. Furthermore, the fillers create voids in the elastomer that destroy the elastomer properties and can be seen as a decrease in G'. If the concentration of fillers is low, the properties of the particle network formed in the composite exceed destruction in the elastomer network and G' increases. However, when filler concentration becomes too high, elastomer destruction exceeds the properties of the particle network and G' of the composite decreases.

5.2.2 Covalent modified carbon nanotubes

By modifying the CNT surface, attraction forces between the CNTs are lowered and the CNTs will not agglomerate to the same extent, which ultimately will improve dispersion.

Functionalised CNTs (f-CNTs) are used as created by the procedure described below. CNTs are functionalised by grafting poly(methacryloyl polydimethylsiloxane) to the CNT surface. The MWCNTs are dispersed in a mixture of anisole and toluene by employing ultrasonication. Azobisisobutyronitrile (AIBN) and alpha-methacryloyl

polydimethylsiloxane are added to the dispersed MWCNT, and free radical polymerisation is conducted in the media. The mixture is then isolated by precipitating into methanol, followed by filtration using a 0.4 mm filter, resulting in a greasy black solid. The product is then used without any further purification. The process gives rise to poly(methacryloyl polydimethylsiloxane) that is both free in solution and covalently grafted to the surface of the MWCNT. From thermal gravimetric analysis (TGA) it is determined that 4% of the poly(methacryloyl polydimethylsiloxane) is grafted onto the CNTs and the rest remains free in the solution.

Samples are prepared with different f-CNT loadings, and conductivities are measured and shown in Figure 35.

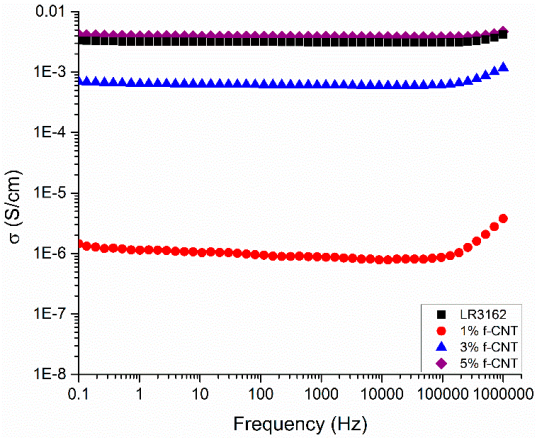

Figure 35 Conductivities of samples with different loadings of functionalised CNTs dispersed in PDMS at room temperature.

As expected, conductivity increases in line with increasing concentrations of CNTs. Upon comparing the conductivity of f-CNT with CNT/IL composites, it is clear that f-CNT has higher conductivities at the same concentrations. For 1 wt% loadings, conductivity increases by a decade and with 3 wt% loading the increase is two decades.

To evaluate the resulting mechanical properties of the f-CNT composites, viscoelastic properties are investigated and depicted in Figure 36.

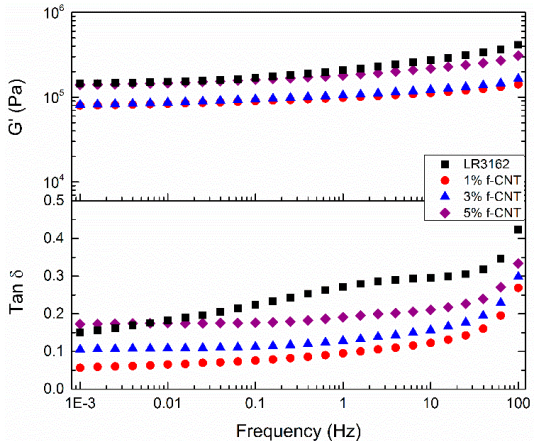

Figure 36 Linear viscoelastic characterisation of samples with different f-CNT loadings at room temperature.

For low concentrations of f-CNTs (1–3 wt%), elastic properties are comparable with the ultrasonicated CNT/IL samples. However, the losses have decreased, which indicates better dispersion. At loadings of 5 wt% G' increases and Tan δ decreases, indicating that the network has not been destroyed and higher loadings are applicable.
It is evident that even at low functionalisation degrees, the increase in conductivity is substantial. Furthermore, to investigate the conductivity and the mechanical properties of samples with a higher amount of poly(methacryloyl polydimethylsiloxane) grafted onto the CNTs, optimisation of the grafting process is needed.

5.3 Conclusion

To ease the dispersion of CNTs, two approaches are investigated. In the first approach, an IL is used as a dispersion agent, and two dispersion methods, ultrasonication and roll milling, are investigated. Conductivities increase in line with increasing concentrations for both dispersion methods. However, conductivity decreases at 5 wt% loading for a 1:1 ratio, indicating that the CNT/IL forms agglomerates. Rheological measurements show the composite getting softer and losses increasing, thereby indicating network destruction. IL concentration is increased to a 1:2 weight ratio and the CNTs are dispersed by ultrasonication. It is observed that the decline in conductivity starts at lower CNT concentrations. Furthermore, network destruction also starts at lower concentrations for higher IL concentrations. For roll milling, conductivity increases in line with increasing concentrations of CNT for the samples without IL, and for the samples containing IL,

conductivity decreases for the sample containing 5 wt% CNT, confirming that by adding IL to the composite the loading limit for the polymer network is reached.

In the second approach CNTs are covalently grafted with poly(methacryloyl polydimethylsiloxane) onto the CNT surface. Functionalising the CNTs before dispersing them in the elastomer matrix eases dispersion, and conductivities are comparable with the commercially available Elastosil LR3162 and increases substantially, compared to the ultrasonication method even with a low degree of functionalisation. Furthermore, at 5 wt% loading, conductivity increases and the network is not destroyed.

6. Conclusion and outlook

6.1 Conclusion

The overall objective of this Ph.D. thesis was to optimise the current large-scale fabrication of DE transducers. The project focused on two parts of the process. The first part investigated an alternative process where microstructures were imprinted onto the surface of DE films using a hot-embossing method. The parameters in which the embossing was performed, such as material hardness, time to perform the embossing and sample thickness, were investigated. Curing profiles were then recorded, in order to determine the gel points.

The embossing was performed for samples with different stoichiometries, and the results showed that they could all be embossed. Moreover, when the material became softer, embossing was performed later – after the gel point – and the embossing window grew larger. Embossing was determined to be performed after the gel point, and the time interval for embossing was 10-25 minutes after the gel point for r=1.2, 15-30 minutes after for r=1.0 and 30-60 after the gel point for r=0.8. Moreover, due to the elastic effects caused by the extra material, it can be concluded that thin films are most favourable for the embossing process.

The second part involved adhering multiple DE layers for the preparation of monolithic elements. Different adhesion configurations were made possible due to the design of the DE films produced by DPP, and different approaches were investigated. For the B2B configuration, where PDMS surfaces were adhered together, two approaches were explored. Adding an aminosilane as an adhesion agent showed that the laminates became slightly stiffer and more fragile as tear strength decreased. Therefore, plasma-treating PDMS surfaces and adhering to laminates was attempted next. The obtained results show that plasma treatment is a suitable method and provides high-strength laminates performing as monolithic elements. Furthermore, the addition of an adhesion agent or additional dielectric material is eliminated, and the thickness of the element is only dependent on the thickness of the DE films.

For the F2B and F2F configurations, conductive fillers were added to an elastomer matrix. Elastosil RT625 was used as the elastomer matrix, due to its adhesion ability. One approach involved adding EG to a PDMS matrix to increase dielectric permittivity.

Furthermore, the elastomer network was reinforced by using an 8-functional crosslinker. The results show that even at low concentrations, EG influences the overall performance of the reinforced elastomer matrix, indicating that increasing the concentration further to make conductive elastomers will increase dielectric losses and the material will get softer due to two-dimensional curing.

The second approach for the F2B and F2F configurations was to use CNTs as fillers for the preparation of conductive elastomers. Three different dispersion methods were investigated. Two methods involved using the CNTs as received and then adding ILs to ease dispersion, while the third method involved modifying the CNTs by covalently grafting poly(methacryloyl polydimethylsiloxane) onto the surface of the CNTs. Ultrasonication and roll milling CNTs with ILs showed that conductivity increased in line with increasing concentrations of CNTs. However, conductivity decreased when CNT concentration exceeded 4 wt% for both dispersion methods. Better dispersion was achieved by roll milling the CNTs, which was seen in the form of higher conductivities at a given concentration. The prepared composites were compared with a commercially available conductive elastomer, Elastosil LR3162, and higher conductivities were achieved at significantly lower filler concentrations.

Functionalising the CNTs before dispersing them in the elastomer matrix eases dispersion, and conductivities are comparable with commercially available Elastosil LR3162 even with a low degree of functionalisation, which indicates that at higher functionalisation degrees conductivities can be increased significantly.

6.2 Future work

The work presented in this thesis provides the foundations for further research and investigation. Firstly, the actuation strain of the plasma-treated laminates should be measured in order to determine and compare the actuation response to single films. Secondly, it would be interesting to determine the adhesion strength of the prepared conductive elastomers to determine if the laminates would detach during operation. To increase conductivity at a given concentration it would be desirable to align the CNTs in the matrix, for example by connecting to an electrical circuit current running through the material while curing. Another interesting approach would be to prepare conductive elastomers using different fillers, such as AgNW, or conductive polymers, such as polyaniline (PANI) and poly(3,4-ethylenedioxythiophene) (PEDOT) in a PDMS matrix. A

second approach might involve changing the matrix to a conductive elastomer and adding conductive filler to increase conductivity further.

Finally, it would be interesting to implement the studied configurations (B2B and F2F) in an element and then adhere multiple layers and investigate the electrical breakdown strength, lifetime and overall performance of a transducer.

7. Experimental work

7.1 Equipment and parameters

7.1.1 Rheological characterisation

Rheological characterisation is performed on either a TA Instrument AR2000 rheometer or an ARES G2 rheometer from TA Instruments, with parallel plate geometry with a diameter of 25 mm and a controlled strain of 2%. The measurements are performed in the frequency range 100-0.01 Hz and with a normal force of 6-8 N.

7.1.2 Electrical breakdown strength

An in-house-built device based on international standards (IEC 60243-1 (1998) and IEC 60243-2 (2001)) is used to measure electrical breakdown strength. Sample thickness is calculated by weighing. The sample is placed between two spherical electrodes and the distance is set to the sample thickness on a digital indicator with a 0.001 mm resolution. A stepwise increase in the voltage (50-100 V/step) at a rate of 0.5-1 steps/s is applied at the point of contact[48], and electrical breakdown strength is measured as the voltage at which the elastomer breaks down and short-circuits. Electrical breakdown strength is measured at 12 points for each sample, and an average of the measurements is indicated as the breakdown strength of the sample.

7.1.3 Peel force

For peel measurements, a Zwick/Roell zmart.pro material tester is used. The sample (130 mm * 25 mm) is attached to a metal plate. The laminate is separated at one end at a distance of approximately 25 mm, and the free end is then clamped to a gripper. The metal plate with the attached sample is fixed to a second gripper. The device will then move the gripper up and the force used to peel the films from one another is measured. The laminate is separated at a 180° angle and a separation rate of 152 mm/min.

7.1.4 Plasma treatment

Plasma treatment is performed using a Plasmatreat RD1004 attached with a nozzle head 22892 acquired from Plasmatreat GmbH, Germany. This nozzle has a working diameter of 55 mm.

A sample is placed on a lift table, so the distance to the nozzle can be adjusted. A moving unit is attached to the lift table that regulates the speed at which the plasma treater moves across the sample.

7.1.5 Actuation

An in-house-built device is used for measuring the actuation of the samples. A sample (60 mm * 20 mm) is fixed on frames and an area of 20 mm * 20 mm is smeared with carbon grease. Conductive electrode tape is attached to the sample, ensuring it is in contact with the carbon grease, to make contact with the high-voltage AC amplifier. The sample is mounted with the clamps on a moveable stage controlled by a c-863 DC motor. The top clamp has a 1kg load cell attached to measure the force the film exerts when actuated at different applied voltages. The measurements are carried out at various applied voltages in the interval 1-5 kV, and the samples are subjected to a 10% pre-stretch.

7.1.6 Conductivity

Conductivity measurements are taken on a broadband dielectric spectrometer, from Novocontrol GmbH, in the frequency range 10^6-0.01 Hz. The samples have a diameter of 20 mm and are 1 mm thick.

7.2 Materials and procedures

7.2.1 Macro-embossing elastomer film

Materials

Samples are prepared by using vinyl-terminated PDMS (DMS-V35 – 49500 g/mole), a 4-functional crosslinker (Tetrakis(dimethyl)silane–328 g/mole) and silicium dioxide treated with hexamethyldizilizane nanoparticles purchased from Gelest Inc. The platinum catalyst (platinum cyclovinylmethyl-siloxane complex, 511) was provided by Hanse Chemie AG, and PDMS oil (Powersil® fluid TR50) was acquired from Wacker Chemie AG.

Procedure

The sample is prepared by weighing the required amounts of all the materials. The premix containing the platinum catalyst is weighed first, and the premix with the crosslinker is weighed last, since the network begins to form when they come into contact. When all the materials have been weighed the sample is mixed with a mechanical stirrer for 2 minutes and put into a vacuum to remove any air bubbles.

When the sample is removed from the vacuum, it can be applied to a film or used for the curing profile.

To ensure macro structuring, a sample of approximately 30 g is made which is then applied to a release liner that is fixed on the table. A framework is fastened to the release liner so that the film reaches the right thickness.

If the newly formed film contains bubbles they are punctured with a needle. The roller is a handle with a detachable wheel with indentations of different patterns. The macrostructure is made with the structured roller by rolling the roller from bottom to top, while embossing is performed at room temperature.

7.2.2 Monolithic PDMS laminates for dielectric elastomer transducers via open-air plasma treatment

Materials

Elastosil LR3043/30 was purchased from Wacker Chemie AG, Germany. Elastosil LR3043/30 is a two-component system in which component A contains vinyl-terminated polydimethylsiloxane (PDMS) and a platinum catalyst, and component B contains a PDMS crosslinker and vinyl-terminated PDMS, amongst others.

Procedure

The elastomer (LR3043/30) is applied in a thin layer onto a carrier web and is subsequently cured in an oven[90]. It is then kept on the carrier web to form a smooth surface without wrinkles and to ease handling. Samples of 20 cm by 20 cm are prepared at distances away from the nozzle ranging from 5 mm to 15 mm in 5 mm increments and speeds in intervals of 5 m/min to 20 m/min in 5 m/min increments.

7.2.3 Design of an elastomer structure to incorporate expanded graphite in silicones, without compromising electromechanical integrity

Materials

The samples are prepared by using PDMS (polydimethylsiloxane – DMS-V35 – 49500 g/mol) and an 8-functional crosslinker (methylhydrosiloxane-dimethylsiloxane copolymer-HMS-301- 1900-2000 g/mol), both purchased from Gelest Inc. The inhibitor (Pt88) and the platinum catalyst (platinum cyclovinylmethyl-siloxane complex, 511) were provided by Hanse Chemie AG. The graphite used in this design was commercially available expanded graphite TIMREX® BNB90, supplied by Timcal. The size distribution of the particles was reported by the supplier as being 50% of the graphite below 36 μm and 90% below 85 μm, with a specific surface area of 28.4 m2/g. The benchmark silicone elastomer was commercially available Elastosil RT625, purchased from Wacker Chemie AG.

In order to prepare the samples a Speedmixer™ was used. The Speedmixer™ from Flack Tek Inc. is a dual asymmetric centrifuge (DAC) 10 FVZ-K, which operates in intervals ranging from 300 to 3500 rpm. The preparation of the 200 μm thick films was performed on an Elcometer 4340 automatic film applicator.

Procedure

The process for preparing the samples was simplified by making premixes. Premix A contained vinyl-terminated PDMS (DMS-V35, 49.67 g, 2 mmol end groups) and an 8-functional crosslinker (HMS-301, 1.72 g, 6 mmol reactive groups), and Premix B contained vinyl-terminated PDMS (DMS-V35, 50 g, 2.02 mmol end groups) and a platinum catalyst (2.04 mg).

Premixes A and B were combined in a Speedmixer cup, and the expanded graphite was added in various concentrations (2-4g, depending on the desired concentration (wt%)). The samples were mixed for 5 minutes at 2750 rpm and then poured into a mould or applied to a release liner and cured in an oven for 14 hours at 80°C.

7.2.4 Dispersion of carbon nanotubes in PDMS and its influence on electrical and mechanical properties

Materials

MWCNTs (NC7000) were purchased from Nanocyl S.A. (Belgium). The size of the MWCNTs is reported by the supplier as being an average diameter of 9.5nm, an average length of 1.5 μm and a surface area of 250-300 m2/g.

The ionic liquid, 1-ethyl-3-methyl imidazolium bis (triflouromethanesulfonyl)imide and heptane, were acquired from Sigma Aldrich.

Elastosil RT625 and the inhibitor PT-88 were purchased from Wacker Chemie AG (Germany). Elastosil RT625 is a two-component system, in which component A consists of vinyl-terminated PDMS and a crosslinker, and component B consists of vinyl-terminated PDMS and a catalyst, among other components such as fillers and additives. The two components are mixed in a 9:1 ratio (A:B).

In order to prepare the samples the zero volt ionizer from Desco Industries Inc., an ultrasonic device UP200S from Heilscher, a mechanical mixer Eurostar from IKA Labortechnik, a rotary-evaporator Laborota 4003 from Heidolph, a Speedmixer™ from Flack Tek Inc. and a three-roll mill from EXAKT Advanced Technologies GmbH are used.

Procedure

For samples containing IL, the CNTs and IL in the desired ratio were weighed in a mortar and ground with a pestle until gelation was observed.

In the first procedure, the CNTs or the CNT/IL mixture was dispersed in heptane at 1 mg CNT/mL and ultrasonicated for 14 minutes in 2 minute intervals. After ultrasonication, component A of Elastosil RT625 was added and the mixture was mechanically mixed for 6 hours at 900 rpm. The heptane was evaporated from the CNT/PDMS or CNT/IL/PDMS mixture using a rotary-evaporator. Component B of Elastosil RT625 was added to the mixture. The final mixture was speed-mixed for 5 minutes at 2750 rpm and cast onto a glass plate with a 1 mm-thick frame, following which another glass plate was placed on top of the sample, thus sandwiching the sample. The glass plates were clamped together and the sample was cured in the oven for 10 minutes at 115°C.

In the second procedure the CNTs or CNT/IL gels, as well as both Elastosil RT625 components, were weighed and the mixture was speed mixed. A 1 wt% inhibitor with respect to the PDMS was added to delay the curing process. The mixture was then speed-mixed for 5 minutes at 2750 rpm and was ready to be dispersed in the roll mill. The gap between the first and second rolls was set to 30 μm, while the gap between the second and third rolls was set to 15 μm and the speed of the third roll was set to 100 rpm. The sample was roll-milled six times until the mixture was uniformly blended.

In the third procedure, the functionalised CNTs were speed-mixed with both components of the PDMS at 2750 rpm for 5 minutes. The sample was then cast on a glass plate and cured in an oven for 10 minutes at 115°C.

References

[1] Zhang, X., Löwe, C., Wissler, M., Jähne, B., and Kovacs, G., 2005, "Dielectric elastomers in actuator technology," Adv. Eng. Mater., **7**(5), pp. 361–367.

[2] Bar-Cohen, Y., 2004, Electroactive polymer (EAP) actuators as artificial muscles: reality, potential, and challenges, SPIE Press, Bellingham, Washington USA.

[3] Pelrine, R., Kornbluh, R., Pei, Q., and Joseph, J., 2000, "High-speed electrically actuated elastomers with strain greater than 100%," Science, **287**, pp. 836–839.

[4] Asaka, K., Mukai, K., Sugino, T., and Kiyohara, K., 2013, "Ionic electroactive polymer actuators based on nano-carbon electrodes," Polym. Int., **62**, pp. 1263–1270.

[5] Immerstrand, C., Holmgren-Peterson, K., Magnusson, K.-E., Jager, E., Krogh, M., Skoglund, M., Selbing, A., and Inganäs, O., 2002, "Conjugated-polymer micro- and milliactuators for biological applications," MRS Bull., **27**, pp. 461–464.

[6] Martinez, J. G., Otero, T. F., and Jager, E. W. H., 2014, "Effect of the electrolyte concentration and substrate on conducting polymer actuators," Langmuir, **30**, pp. 3894–3904.

[7] Persson, K. M., Karlsson, R., Svennersten, K., Löffler, S., Jager, E. W. H., Richter-Dahlfors, A., Konradsson, P., and Berggren, M., 2011, "Electronic control of cell detachment using a self-doped conducting polymer," Adv. Mater., **23**, pp. 4403–4408.

[8] Kim, K. J., and Shahinpoor, M., 2002, "A novel method of manufacturing three-dimensional ionic polymer-metal composites (IPMCs) biomimetic sensors, actuators and artificial muscles," Polymer, **43**, pp. 797–802.

[9] Zamani, S., and Nemat-Nasser, S., 2004, "Controlled actuation of Nafion-based ionic polymer-metal composites (IPMCs) with ethylene glycol as solvent," Proc. SPIE, **5385**, pp. 159–163.

[10] O'Halloran, A., O'Malley, F., and McHugh, P., 2008, "A review on dielectric elastomer actuators, technology, applications, and challenges," J. Appl. Phys., **104**(7), p. 071101.

[11] Zakaria, S., Morshuis, P. H. F., Benslimane, M., Gernaey, K. V, and Skov, A. L., 2014, "The electrical breakdown of thin dielectric elastomers: thermal effects," Proc. SPIE, **9056**, p. 90562V.

[12] Jean-Mistral, C., Sylvestre, A., Basrour, S., and Chaillout, J.-J., 2010, "Dielectric properties of polyacrylate thick films used in sensors and actuators," Smart Mater. Struct., **19**(7), p. 075019.

[13] Kofod, G., Kornbluh, R., Pelrine, R., and Sommer-Larsen, P., 2001, "Actuation response of polyacrylate dielectric elastomers," Proc. SPIE, **4329**, pp. 141–147.

[14] Jo, N.-J., Lim, D.-H., Bark, G.-M., Chun, H.-H., Lee, I.-W., and Park, H., 2010, "Polyurethane-based actuators with various polyols," J. Mater. Sci. Technol., **26**(8), pp. 763–768.

[15] Jung, Y., Park, H., Jo, N., and Jeong, H., 2007, "Fabrication and performance evaluation of diaphragm-type polymer actuators using segmented polyurethane according to chemical-hard-segment content," Sensors Actuators A Phys., **136**, pp. 367–373.

[16] Ueda, T., Kasazaki, T., Kunitake, N., Hirai, T., Kyokane, J., and Yoshino, K., 1997, "Polyurethane elastomer actuator," Synth. Met., **85**, pp. 1415–1416.

[17] Yang, D., Tian, M., Dong, Y., Liu, H., Yu, Y., and Zhang, L., 2012, "Disclosed dielectric and electromechanical properties of hydrogenated nitrile–butadiene dielectric elastomer," Smart Mater. Struct., **21**(3), p. 035017.

[18] Jung, K., Lee, J., Cho, M., Koo, J. C., Nam, J., Lee, Y., and Choi, H. R., 2007, "Development of enhanced synthetic elastomer for energy-efficient polymer actuators," Smart Mater. Struct., **16**(2), pp. S288–S294.

[19] Cheng, Z., Bharti, V., Xu, T., Xu, H., Mai, T., and Zhang, Q. M., 2001, "Electrostrictive poly (vinylidene fluoride-trifluoroethylene) copolymers," Sensors Actuators A, **90**, pp. 138–147.

[20] Benslimane, M. Y., Kiil, H.-E., and Tryson, M. J., 2010, "Dielectric electro-active polymer push actuators: performance and challenges," Polym. Int., **59**(3), pp. 415–421.

[21] Kussmaul, B., Risse, S., Kofod, G., Waché, R., Wegener, M., McCarthy, D. N., Krüger, H., and Gerhard, R., 2011, "Enhancement of dielectric permittivity and electromechanical response in silicone elastomers: molecular grafting of organic

dipoles to the macromolecular network," Adv. Funct. Mater., **21**(23), pp. 4589–4594.

[22] Skov, A. L., Vudayagiri, S., and Benslimane, M., 2013, "Novel silicone elastomer formulations for DEAPs," **8687**, p. 86871I.

[23] Yu, L., Gonzalez, L. B., Hvilsted, S., and Skov, A. L., 2014, "Soft silicone based interpenetrating networks as materials for actuators," Proc. SPIE, **9056**, p. 90560C.

[24] Liu, H., Zhang, L., Yang, D., Yu, Y., Yao, L., and Tian, M., 2013, "Mechanical, dielectric, and actuated strain of silicone elastomer filled with various types of TiO2," Soft Mater., **11**(3), pp. 363–370.

[25] Shankar, R., Ghosh, T., and Spontak, R., 2007, "Dielectric elastomers as next-generation polymeric actuators," Soft Matter, **3**, pp. 1116–1129.

[26] Kornbluh, R., Pelrine, R., Pei, Q., Heydt, R., Stanford, S., Oh, S., and Eckerle, J., 2002, "Electroelastomers: applications of dielectric elastomer transducers for actuation, generation and smart structures," Proc. SPIE, **4698**, pp. 254–270.

[27] Michel, S., Zhang, X. Q., Wissler, M., Löwe, C., and Kovacs, G., 2009, "A comparison between silicone and acrylic elastomers as dielectric materials in electroactive polymer actuators," Polym. Int., **59**(3), pp. 391–399.

[28] Sommer-Larsen, P., Kofod, G., MH, S., and Benslimane, M., 2002, "Performance of dielectric elastomer actuators and materials," Proc. SPIE, **4695**, pp. 158–166.

[29] Meijer, K., Rosenthal, M. S., and Full, R. J., 2001, "Muscle-like actuators? A comparison between three electroactive polymers," Proc. SPIE, **4329**, pp. 7–15.

[30] Ha, S. M., Wissler, M., Pelrine, R., Stanford, S., Kovacs, G., and Pei, Q., 2007, "Characterization of electroelastomers based on interpenetrating polymer networks," Proc. SPIE, **6524**, pp. 652408 – 1–10.

[31] Vudayagiri, S., Junker, M. D., and Skov, A. L., 2013, "Factors affecting the surface and release properties of thin polydimethylsiloxane films," Polym. J., **45**(8), pp. 871–878.

[32] Kollosche, M., Stoyanov, H., Ragusch, H., Risse, S., Becker, A., and Kofod, G., 2010, "Electrical breakdown in soft elastomers: Stiffness dependence in un-pre-stretched elastomers," 10th IEEE Int. Conf. Solid Dielectr., (3), pp. 1–4.

[33] Carpi, F., and De Rossi, D., 2005, "Improvement of electromechanical actuating performances of a silicone dielectric elastomer by dispersion of titanium dioxide powder," IEEE Trans. Dielectr. Electr. Insul., **12**(4), pp. 835–843.

[34] Ouyang, G. M., Wang, K. Y., and Chen, X. Y., 2011, "Enhanced electro-mechanical performance of TiO_2 nano-particle modified polydimethylsiloxane (PDMS) as electroactive polymers," 16th Int. Solid-State Sensors, Actuators Microsystems Conf., pp. 614–617.

[35] Zhao, H., Wang, D.-R., Zha, J.-W., Zhao, J., and Dang, Z.-M., 2013, "Increased electroaction through a molecular flexibility tuning process in TiO2–polydimethylsilicone nanocomposites," J. Mater. Chem. A, **1**(9), p. 3140.

[36] Cazacu, M., Ignat, M., Racles, C., Cristea, M., Musteata, V., Ovezea, D., and Lipcinski, D., 2013, "Well-defined silicone-titania composites with good performances in actuation and energy harvesting," J. Compos. Mater., **48**(13), pp. 1533–1545.

[37] Stoyanov, H., Brochu, P., Niu, X., Della Gaspera, E., and Pei, Q., 2012, "Dielectric elastomer transducers with enhanced force output and work density," Appl. Phys. Lett., **100**(26), p. 262902.

[38] Lotz, P., Matysek, M., Lechner, P., Hamann, M., and Schlaak, H. F., 2008, "Dielectric elastomer actuators using improved thin film processing and nanosized particles," Proc. SPIE, **6927**, pp. 692723 – 1–10.

[39] Yu, L., Vudayagiri, S., Zakaria, S., Benslimane, M. Y., and Skov, A. L., 2014, "Filled liquid silicone rubbers: possibilities and challenges," Proc. SPIE, **9056**, p. 90560S.

[40] Szabo, J. P., Hiltz, J. A., Cameron, C. G., Underhill, R. S., Massey, J., White, B., Leidner, J., Scotia, N., Materials, B., and Canada, T., 2003, "Elastomeric composites with high dielectric constant for use in Maxwell stress actuators," Proc. SPIE, **5051**, pp. 180–190.

[41] Khastgir, D., and Adachi, K., 1999, "Piezoelectric and dielectric properties of siloxane elastomers filled with bariumtitanate," J. Polym. Sci. Part B Polym. Phys., **37**(21), pp. 3065–3070.

[42] Liu, Y., Liu, L., Zhang, Z., and Leng, J., 2009, "Dielectric elastomer film actuators: characterization, experiment and analysis," Smart Mater. Struct., **18**(9), p. 095024.

[43] Madsen, F. B., Dimitrov, I., Daugaard, A. E., Hvilsted, S., and Skov, A. L., 2013, "Novel cross-linkers for PDMS networks for controlled and well distributed grafting of functionalities by click chemistry," Polym. Chem., **4**(5), pp. 1700–1707.

[44] Madsen, F. B., Daugaard, A. E., Hvilsted, S., Benslimane, M. Y., and Skov, A. L., 2013, "Dipolar cross-linkers for PDMS networks with enhanced dielectric permittivity and low dielectric loss," Smart Mater. Struct., **22**(10), p. 104002.

[45] Madsen, F. B., Egede Daugaard, A., Hvilsted, S., and Skov, A. L., 2013, "Novel silicone compatible cross-linkers for controlled functionalization of PDMS networks," proc. SPIE, **8687**, pp. 86871H – 1–13.

[46] Madsen, F. B., Yu, L., Daugaard, A. E., Hvilsted, S., and Skov, A. L., 2014, "Silicone elastomers with high dielectric permittivity and high dielectric breakdown strength based on dipolar copolymers," Polymer, **55**(24), pp. 6212–6219.

[47] Madsen, F. B., Javakhishvili, I., Jensen, R. E., Daugaard, A. E., Hvilsted, S., and Skov, A. L., 2014, "Synthesis of telechelic vinyl/allyl functional siloxane copolymers with structural control," Polym. Chem., **5**(24), pp. 7054–7061.

[48] Kiil, H.-E., and Benslimane, M., 2009, "Scalable industrial manufacturing of DEAP," Proc. SPIE, **7287**, pp. 72870R – 1–10.

[49] Benslimane, M., Gravesen, P., and Sommer-Larsen, P., 2002, "Mechanical properties of dielectric elastomer actuators with smart metallic compliant electrodes," Proc. SPIE, **4695**, pp. 150–157.

[50] Vudayagiri, S., and Skov, A. L., 2014, "Methods to ease the release of thin polydimethylsiloxane films from difficult substrates," Polym. Adv. Technol., **25**(3), pp. 249–257.

[51] Carpi, F., Migliore, A., Serra, G., and De Rossi, D., 2005, "Helical dielectric elastomer actuators," Smart Mater. Struct., **14**, pp. 1–7.

[52] Carpi, F., Salaris, C., and De Rossi, D., 2007, "Folded dielectric elastomer actuators," Smart Mater. Struct., **16**(2), pp. S300–S305.

[53] Eddings, M. A., Johnson, M. A., and Gale, B. K., 2008, "Determining the optimal PDMS–PDMS bonding technique for microfluidic devices," J. Micromechanics Microengineering, **18**(6), p. 067001.

[54] Penskiy, I., Gerratt, A. P., and Bergbreiter, S., 2011, "Friction, adhesion and wear properties of PDMS films on silicon sidewalls," J. Micromechanics Microengineering, **21**(10), p. 105013.

[55] Unger, M. A., Chou, H.-P., Thorsen, T., Scherer, A., and Quake, S. R., 2000, "Monolithic Microfabricated Valves and Pumps by Multilayer Soft Lithography," Science, **288**(5463), pp. 113–116.

[56] Yu, L., Daugaard, A. E., and Skov, A. L., 2012, "Adhesion between polydimethylsiloxane layers by crosslinking," Adv. Sci. Technol., **79**, pp. 47–52.

[57] Yu, L., and Skov, A. L., 2014, "Monolithic growth of partly cured polydimethylsiloxane thin film layers," Polym. J., **46**(2), pp. 123–129.

[58] Satyanarayana, S., Karnik, R. N., and Majumdar, A., 2005, "Stamp-and-stick room-temperature bonding technique for microdevices," J. Microelectromechanical Syst., **14**(2), pp. 392–399.

[59] Ginn, B. T., and Steinbock, O., 2003, "Polymer surface modification using microwave-oven-generated plasma," Langmuir, **19**, pp. 8117–8118.

[60] McDonald, J. C., and Whitesides, G. M., 2002, "Poly(dimethylsiloxane) as a material for fabricating microfluidic devices.," Acc. Chem. Res., **35**(7), pp. 491–9.

[61] Rosset, S., and Shea, H. R., 2012, "Flexible and stretchable electrodes for dielectric elastomer actuators," Appl. Phys. A, **110**(2), pp. 281–307.

[62] Stoyanov, H., Kollosche, M., Risse, S., Waché, R., and Kofod, G., 2013, "Soft conductive elastomer materials for stretchable electronics and voltage controlled artificial muscles.," Adv. Mater., **25**(4), pp. 578–83.

[63] Hansen, T. S., West, K., Hassager, O., and Larsen, N. B., 2007, "Highly stretchable and conductive polymer material made from Poly(3,4-ethylenedioxythiophene) and polyurethane elastomers," Adv. Funct. Mater., **17**(16), pp. 3069–3073.

[64] Liang, H.-W., Guan, Q.-F., Zhu, Z.-, Song, L.-T., Yao, H.-B., Lei, X., and Yu, S.-H., 2012, "Highly conductive and stretchable conductors fabricated from bacterial cellulose," NPG Asia Mater., **4**(6), pp. 1–6.

[65] Korte, K. E., Skrabalak, S. E., and Xia, Y., 2008, "Rapid synthesis of silver nanowires through a CuCl- or CuCl2-mediated polyol process," J. Mater. Chem., **18**(4), pp. 437–441.

[66] Sun, Y., Gates, B., Mayers, B., and Xia, Y., 2002, "Crystalline silver nanowires by soft solution processing," Nano Lett., **2**(2), pp. 165–168.

[67] Akter, T., and Kim, W. S., 2012, "Reversibly stretchable transparent conductive coatings of spray-deposited silver nanowires," ACS Appl. Mater. Interfaces, **4**, pp. 1855–1859.

[68] Yun, S., Niu, X., Yu, Z., Hu, W., Brochu, P., and Pei, Q., 2012, "Compliant silver nanowire-polymer composite electrodes for bistable large strain actuation.," Adv. Mater., **24**(10), pp. 1321–7.

[69] Seo, D. K., Kang, T. J., Kim, D. W., and Kim, Y. H., 2012, "Twistable and bendable actuator: a CNT/polymer sandwich structure driven by thermal gradient.," Nanotechnology, **23**(7), p. 075501.

[70] Moniruzzaman, M., and Winey, K. I., 2006, "Polymer nanocomposites containing carbon nanotubes," Macromolecules, **39**, pp. 5194–5205.

[71] Ebbesen, T. W., 1994, "Carbon nanotubes," Annu. Rev. Mater. Sci., **24**(1), pp. 235–264.

[72] Ajayan, P. M., 1999, "Nanotubes from carbon," Chem. Rev., **99**(7), pp. 1787–1800.

[73] Bokobza, L., 2007, "Multiwall carbon nanotube elastomeric composites: A review," Polymer, **48**(17), pp. 4907–4920.

[74] Subramaniam, K., Das, A., Stöckelhuber, K. W., and Heinrich, G., 2013, "Elastomer composites based on carbon nanotubes and ionic liquid," Rubber Chem. Technol., **86**(3), pp. 367–400.

[75] Peng, R., Wang, Y., Tang, W., Yang, Y., and Xie, X., 2013, "Progress in imidazolium ionic liquids assisted fabrication of carbon nanotube and graphene polymer composites," Polymers, **5**(2), pp. 847–872.

[76] Ajayan, P. M., and Tour, J. M., 2007, "Nanotube composites," Nature, **447**, pp. 1066–1068.

[77] Fritzsche, J., Lorenz, H., and Klüppel, M., 2009, "CNT based elastomer-hybrid-nanocomposites with promising mechanical and electrical properties," Macromol. Mater. Eng., **294**(9), pp. 551–560.

[78] Gojny, F. H., and Schulte, K., 2004, "Functionalisation effect on the thermo-mechanical behaviour of multi-wall carbon nanotube/epoxy-composites," Compos. Sci. Technol., **64**, pp. 2303–2308.

[79] Ramanathan, T., Liu, H., and Brinson, L. C., 2005, "Functionalized SWNT/polymer nanocomposites for dramatic property improvement," J. Polym. Sci. Part B Polym. Phys., **43**, pp. 2269–2279.

[80] Wu, H.-L., Yang, Y., Ma, C. M., and Kuan, H., 2005, "Molecular mobility of free-radical-functionalized carbon-nanotube/siloxane/poly (urea urethane) nanocomposites," J. Polym. Sci. Part A Polym. Chem., **43**, pp. 6084–6094.

[81] Fukushima, T., Kosaka, A., Ishimura, Y., Yamamoto, T., Takigawa, T., Ishii, N., and Aida, T., 2003, "Molecular ordering of organic molten salts triggered by single-walled carbon nanotubes," Science, **30**, pp. 2072–2074.

[82] Oh, K., Lee, J. Y., Lee, S.-S., Park, M., Kim, D., and Kim, H., 2013, "Highly stretchable dielectric nanocomposites based on single-walled carbon nanotube/ionic liquid gels," Compos. Sci. Technol., **83**, pp. 40–46.

[83] Das, A., Stöckelhuber, K. W., Jurk, R., Fritzsche, J., Klüppel, M., and Heinrich, G., 2009, "Coupling activity of ionic liquids between diene elastomers and multi-walled carbon nanotubes," Carbon, **47**, pp. 3313–3321.

[84] Subramaniam, K., Das, A., Steinhauser, D., Klüppel, M., and Heinrich, G., 2011, "Effect of ionic liquid on dielectric, mechanical and dynamic mechanical properties of multi-walled carbon nanotubes/polychloroprene rubber composites," Eur. Polym. J., **47**(12), pp. 2234–2243.

[85] Steinhauser, D., 2012, "Influence of ionic liquids on the dielectric relaxation behavior of CNT based elastomer nanocomposites," Express Polym. Lett., **6**(11), pp. 927–936.

[86] Likozar, B., 2010, "Diffusion of ionic liquids into elastomer/carbon nanotubes composites and tensile mechanical properties of resulting materials," Sci. Iran., **17**(1), pp. 35–42.

[87] Subramaniam, K., Das, A., Häußler, L., Harnisch, C., Stöckelhuber, K. W., and Heinrich, G., 2012, "Enhanced thermal stability of polychloroprene rubber composites with ionic liquid modified MWCNTs," Polym. Degrad. Stab., **97**(5), pp. 776–785.

[88] Subramaniam, K., Das, A., Simon, F., and Heinrich, G., 2013, "Networking of ionic liquid modified CNTs in SSBR," Eur. Polym. J., **49**(2), pp. 345–352.

[89] Subramaniam, K., Das, A., and Heinrich, G., 2011, "Development of conducting polychloroprene rubber using imidazolium based ionic liquid modified multi-walled carbon nanotubes," Compos. Sci. Technol., **71**(11), pp. 1441–1449.

[90] Larsen, A. L., Hansen, K., Sommer-Larsen, P., Hassager, O., Bach, A., Ndoni, S., and Jørgensen, M., 2003, "Elastic properties of nonstoichiometric reacted PDMS networks," Macromolecules, **36**(26), pp. 10063–10070.

[91] Chambon, F., and Winter, H. H., 1987, "Linear viscoelasticity at the gel point of a crosslinking PDMS with imbalanced stoichiomety," J. Rheol., **31**(8), pp. 683–697.

[92] Jensen, M. K., Bach, A., Hassager, O., and Skov, A. L., 2009, "Linear rheology of cross-linked polypropylene oxide as a pressure sensitive adhesive," Int. J. Adhes. Adhes., **29**(7), pp. 687–693.

[93] Winter, H. H., 1987, "Can the gel point of a cross-linking polymer be detected by the G' - G" crossover," Polym. Eng. Sci., **27**(22), pp. 1698–1702.

[94] Winter, H. H., 1986, "Analysis of linear viscoelasticity of a crosslinking polymer at the gel point," J. Rheol., **30**(2), p. 367.

[95] Hassouneh, S. S., Daugaard, A. E., and Skov, A. L., 2015, "Design of elastomer structure to facilitate incorporation of expanded graphite in silicones without compromising elasticity.", Macromol. Mater. Eng., **300**(5), pp. 542-550.

[96] Zakaria, S., Morshuis, P. H. F., Benslimane, M. Y., Yu, L., and Skov, A. L., 2015, "The electrical breakdown strength of prestretched elastomers with and without sample volume conservation." Submitted to Smart. Mater. Struct., **24**, p.055009

[97] Daugaard, A. E., Hassouneh, S. S., Kostrzewska, M., Bejenariu, A. G., and Skov, A. L., 2013, "High-dielectric permittivity elastomers from well-dispersed expanded graphite in low concentrations," Proc. SPIE, **8687**, p. 868729.

[98] Li, M., and Jeong, Y. G., 2011, "Preparation and characterization of high-performance poly(trimethylene terephthalate) nanocomposites reinforced with exfoliated graphite," Macromol. Mater. Eng., **296**(2), pp. 159–167.

[99] Wissert, R., Steurer, P., Schopp, S., Thomann, R., and Mülhaupt, R., 2010, "Graphene nanocomposites prepared from blends of polymer latex with chemically reduced graphite oxide dispersions," Macromol. Mater. Eng., **295**(12), pp. 1107–1115.

[100] Cicuta, P., and Hopkinson, I., 2004, "Scaling of dynamics in 2d semi-dilute polymer solutions," Europhys. Lett., **68**, pp. 65–71.

[101] Vudayagiri, S., Zakaria, S., Yu, L., Hassouneh, S. S., Benslimane, M., and Skov, A. L., 2014, "High breakdown-strength composites from liquid silicone rubbers," Smart Mater. Struct., **23**(10), p. 105017.

[102] Masao Doi, 1996, Introduction to Polymer Physics, Oxford University Press, New York.

[103] Barron, R. E., and Fritz, J. S., 1983, "Reproducible preparation of low-capacity anion-exchange resins," React. Polym. Ion Exch. Sorbents, **1**(3), pp. 215–226.

Appendices

Appendix A

S.Hassouneh, S. Vudayagiri, L.Yu, M. Junker, U. Hansen, A. L. Skov, 2012 Fremstilling af dielektriske elektroaktive polymerer i stor skala*, Dansk Kemi*, 93 (10), 22-24.

Fremstilling af dielektriske elektroaktive polymerer i stor skala

Interessen for dielektriske elektroaktive polymerfilm er de seneste år steget markant. For overhovedet at kunne producere de ønskede mængder til en konkurrencedygtig pris er optimering og effektivisering af produktionen af disse film et krav for teknologiens overlevelse.

Af Suzan Hassouneh[1], Sindhu Vudayagiri[1], Liyun Yu[1], Michael Junker[2], Ulrik Hansen[2], Anne Ladegaard Skov[1]
[1]Institut for Kemiteknik, DTU; [2]Danfoss PolyPower A/S

Dielektriske elektroaktive polymerer (DEAP) film fremstilles indtil videre kun på pilotskala, hvor Danfoss PolyPower A/S (DPP) anses for verdens ledende producent. For at DEAP-teknologien kan vinde indpas i så forskellige applikationer som bølgehøstere, ultratynde højtalere, ventiler og effektivisering af vindmøllemængder er det nødvendigt med en effektiv og billig produktion af de tynde polymerfilm og en løbende optimering af DEAP-materialet. Optimeringen af materialeegenskaberne blev drøftet i en foregående artikel [1].

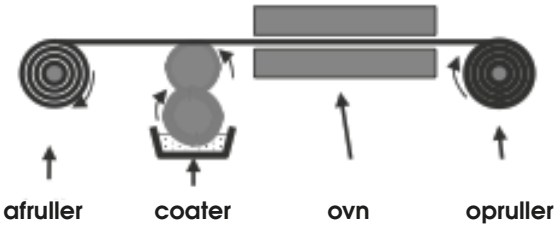

Figur 2. Illustration af trin 2 og 3. Coating og hærdning af elastomeren på en mikrostruktureret carrier web. Coateren påfører den meget viskøse elastomer-blanding til den korrugerede liner i et meget tyndt lag (ca. 50 µm).

Den nuværende proces for fremstillingen af DEAP-film består overordnet set af følgende trin hos DPP:

1. Blanding af en 2-komponent silikone-elastomer og opløsningsmiddel og fjernelse af luftbobler
2. Coating af den flydende elastomer på en struktureret carrier web
3. Hærdning af elastomeren ved opvarmning
4. Aftagning af elastomeren fra carrier web og overførsel til nonwoven liner
5. Elektrodepåførsel vha. metal sputter på struktureret side
6. Aftagning af nonwoven og påførsel af liner
7. Sammenlægning af to spejlvendte film med de ustrukturerede sider mod hinanden

Figur 2 illustrerer trin 2 og 3 i processen, som sammen med trin 4 kan være problematiske og er meget afhængige af mate-

DEAP-applikationer

DEAP-teknologien blev oprindeligt udviklet med kunstige muskler som hovedformål pga. deres evne til at efterligne biologiske muskler. Det skyldes deres elektro-reagerende egenskaber og meget identiske egenskaber med rigtige muskler, hvilket står i stærk kontrast til andre typer af aktuatorer. Det har senere vist sig, at DEAP har en bred industriel og kommerciel anvendelighed.

Figur 1. Forskellige applikationer til DEAP-materialet.

Billede A viser en traditionel højttaler (venstre) sammenlignet med en højttaler af DEAP-materialet (højre), som er væsentlig tyndere end den traditionelle [2].

Billede B viser en tablet for synshandicappede, der dynamisk skifter strukturen på overfladen ved et sæt af pins, som styres af en elektromagnetisk spole, hvor *Braille*-tekst (blindskrift) bliver simuleret [3,4].

På billede C ses et bølgekraftanlæg, der ved hjælp af DEAP-materialet skal kunne optage de uregelmæssige og varierende kræfter fra bølgerne og omforme energien direkte til strøm [5].

På billede D er der vist en aktiv bandage, der har elementer fremstillet af DPPs DEAP-materiale, der kan massere muskelgrupper, støtte blodcirkulationen og give lindring til trætte ben samt forbedre rehabiliteringstiden [6,7].

rialeegenskaberne. Den nuværende proces bevirker også, at det er nødvendigt med tre forskellige linere, nemlig en genbrugelig, men både kostbar og skrøbelig, mikrostruktureret carrier web, en billig nonwoven liner samt en billig liner til opbevaring af DEAP-film på ruller inden endelig montering. Endelig kræver coateprocessen anvendelse af store mængder opløsningsmiddel, hvilket udgør både en miljømæssig samt en økonomisk belastning af det endelige produkt.

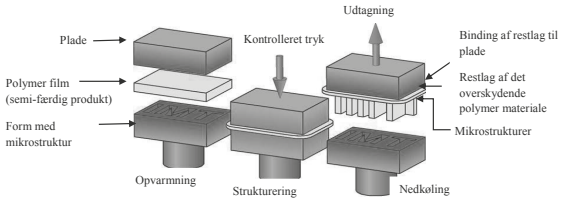

Figur 3. Metode til mikrostrukturering af termoplast.

Elastomer vs. termoplast

Elastomerer er amorfe polymerer, der udviser elasticitet (har evnen til hurtigt at strække og tilbagetrække).

De lange polymerer krydsbinder under hærdningen og danner et netværk. Krydsbindingspunkter sikrer materialets stabilitet ved alle temperaturer op til dekompositionstemperaturen, som for silikone er langt over 400°C.

Termoplast er polymerer, som ved opvarmning bliver til en homogeniseret væske, der bliver hård igen ved afkøling. Disse egenskaber er reversible. Dvs. at termoplasten kan opvarmes, omformes og nedkøles flere gange, hvilket betyder at den ofte genbruges.

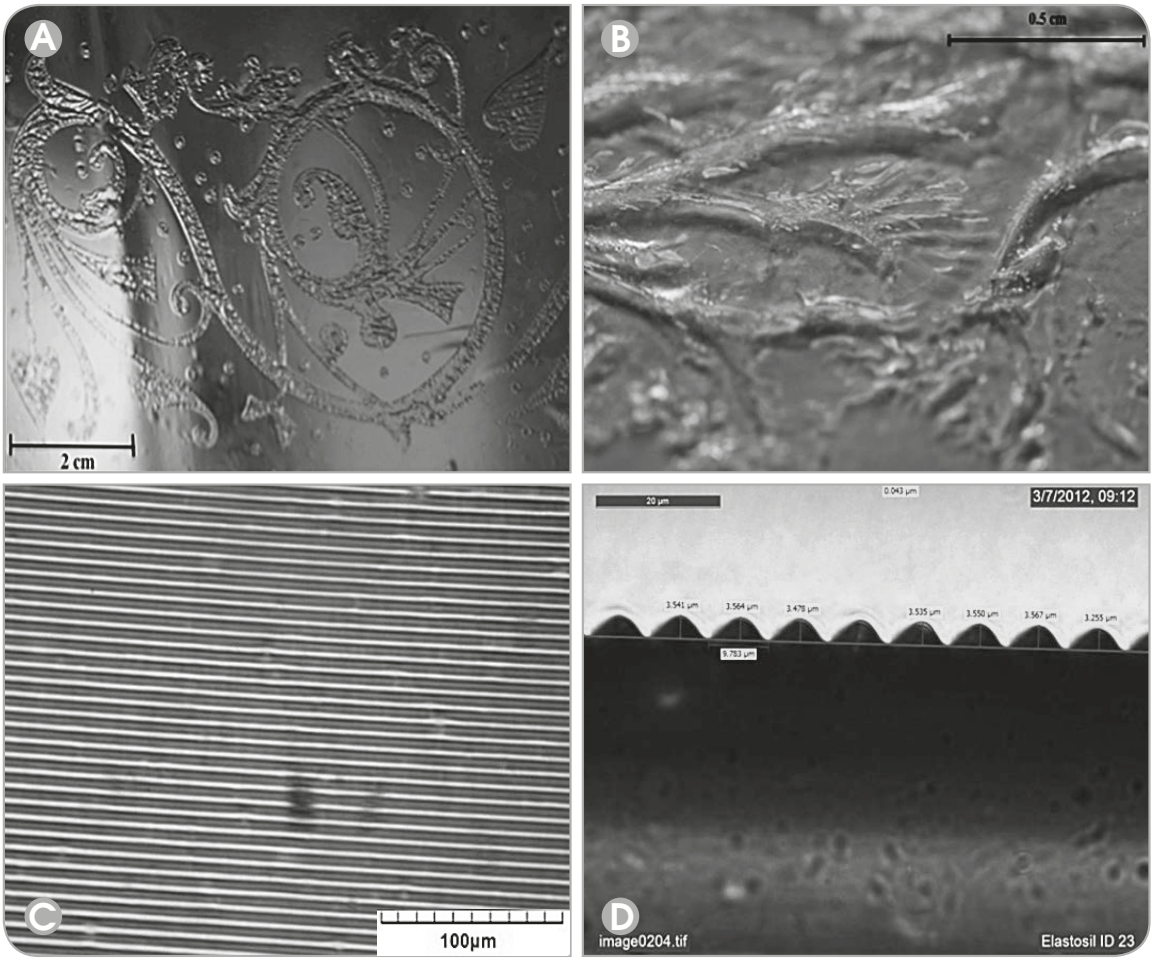

Figur 4. Billeder af struktureringen i både makro- og mikroskala. Billede A viser makrostruktureringen, mens billede B viser fordybningerne i filmen ved makrostruktureringen. Billede C illustrerer mikrostrukturen i overfladen af filmen, og billede D illustrerer filmens tværsnit, og dimensionerne af mikrostrukturen.

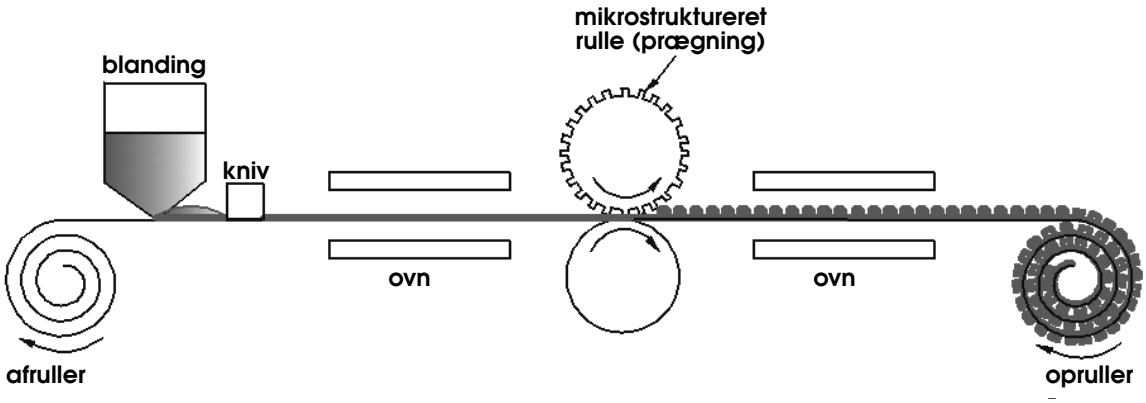

Figur 5. Alternativ metode til fremstilling af DEAP-materialet, hvor prægning af filmen sker ved anvendelse af en mikrostruktureret rulle i en kontinuert proces.

Optimering af processen

For at komme disse problematikker til livs, skal processen optimeres. En måde at optimere processen på er at anvende en metode, der er udviklet og anvendes til termoplastiske polymerer, hvor mikrostrukturen almindeligvis bliver påtrykt ved hot embossing (varmeprægning) teknologi, som det ses på figur 3.

Teknologien er baseret på at opvarme en termoplast-polymer, til den bliver blødgjort og støbes mellem en master metalform med mikrostruktur og en flad plade, der kontrolleret bliver trykket sammen. Derefter nedkøles materialet og kan fjernes fra støbeformen [8].

Denne proces kan også køres kontinuert ved at anvende en opvarmet mikrostruktreret rulle, der rulles på en polymerfilm, hvorefter den strukturerede film nedkøles.

Det er i laboratoriet undersøgt, om det er muligt at anvende metoden analogt til elastomere film. Undersøgelsen/studiet er delt i to, en del hvor elastomerfilmen bliver makrostruktureret, og en del hvor elastomerfilmen bliver mikrostruktureret.

Inden selve prægningen er der lavet hærdeprofiler for at bestemme, hvornår prægningen skal foretages, idet viskositeten af den flydende elastomerblanding ikke må være for lav. Er den det, vil prægningen forsvinde, og elastomeren vil flyde tilbage til sin originale tilstand uden struktur, når den strukturerede rulle fjernes. Er viskositeten derimod for høj, kan man ikke præge filmen, idet elastomeren vil være for elastisk, og enhver påført deformation vil blive presset tilbage af filmens elastiske kræfter.

Når tiden er bestemt, præges filmen. På figur 4 ses der på billederne A og B makrostrukturering af filmene, mens mikrostruktureringen ses på billederne C og D.

Idet det har vist sig muligt at anvende metoden til elastomerer, er en alternativ proces til fremstillingen af DEAP-film:

1. Blanding af en 2-komponent silikone elastomer og fjernelse af luftbobler
2. Coating af den flydende elastomer på en liner
3. Præ-hærdning af elastomeren ved opvarmning
4. Prægning af elastomeren
5. Post-hærdning af elastomeren ved opvarmning
6. Elektrodepåførsel vha. metal sputter på struktureret side
7. Aftagning af liner og påførsel af liner
8. Sammenlægning af to spejlvendte film

Umiddelbart kan den foreslåede proces virke mere kompliceret med totrins hærdning, men man kan forestille sig, at det laves til én integreret enhed sammen med prægningen. Se figur 5 hvor trin 2-5 i processen illustreres. Den problematiske aftagning af elastomeren er ved den foreslåede proces elimineret eller i hvert fald reduceret til et release-problem fra en ikke-struktureret film med et væsentligt mindre overfladeareal, hvilket allerede er løst i andre produktioner af tynde film.

Ved den nye proces kan brugen af nonwoven elimineres, da filmen ved prægning vender rigtigt før elektrodepåførslen. Dvs. at elektroderne, der stabiliserer materialet, påføres før den kritiske proces vedrørende aftagning skal udføres. Der forventes hermed en kraftig reduktion af kasserede produkter ved dette trin.

På længere sigt kan der spares opløsningsmiddel, da en høj viskositet er favorabel for prægning, mens flydeegenskaberne i den tidligere proces skulle være gode for at danne korrugeringerne.

Ovenstående er et godt eksempel på, at det kan være yderst favorabelt – både økonomisk og miljømæssigt – at gentænke processerne af både simple og mere komplicerede produkter.

E-mail-adresse
Anne Ladegaard Skov: al@kt.dtu.dk

Referencer:

1. F. Bahrt Madsen, A. Egede Daugaard, S. Hvilsted, A. Ladegaard Skov. "Udvikling af materialer til kunstige muskler", *Dansk Kemi*, 93, nr. 9, 2012, side 48-51
2. O'Halloran, A., O'Malley, F., & McHugh, P. (2008). A review on dielectric elastomer actuators, technology, applications and challenges. *Applied Physics Reviews - Focused review , 104* (7).
3. http://www.syahdiar.org/eap-braille-ebook/view-braille-book-electronic-device.html
4. http://www.jpl.nasa.gov/news/features.cfm?feature=2278
5. http://hoejteknologifonden.dk/nyheder/nyhedsoversigt/135_mill_kr_skal_udvikle_sundhed_og_skabe_groen_produktion/groen_produktion/
6. http://www.polypower.com/products/Actuators/application-outlook.htm
7. http://www.ohmatex.dk/indhold.php?page_id=50
8. A. Kolew, D. Münch, K. Sikora, and M. Worgull, "Hot embossing of micro and sub-micro structured inserts for polymer replication," *Microsystem Technologies*, vol. 17, no. 4, pp. 609-618, Dec. 2010.

Appendix B

S. S. Hassouneh, A. E. Daugaard, A. L. Skov, 2015, Design of elastomer structure to facilitate incorporation of expanded graphite in silicones without compromising electromechanical integrity, *Macromolecular Materials and Engineering,* **300**(5), 542-550

Design of Elastomer Structure to Facilitate Incorporation of Expanded Graphite in Silicones Without Compromising Electromechanical Integrity

Suzan Sager Hassouneh, Anders Egede Daugaard, Anne Ladegaard Skov*

The development of elastomer materials with a high dielectric permittivity has attracted increased interest over the past years due to their use in, for example, dielectric elastomers. For this particular use, both the electrically insulating properties — as well as the mechanical properties of the elastomer — have to be tightly controlled in order not to destroy favorable elastic properties by the addition of particles. This study focuses on improving the electromechanical properties of an enhanced PDMS matrix with expanded graphite (EG) as filler. The PDMS matrix is crosslinked by means of an 8-functional crosslinker, which allows for development of a suitable network matrix. The dielectric permittivity was increased by almost a factor of 4 compared to a benchmark silicone elastomer.

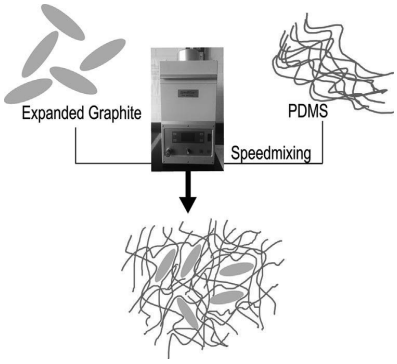

1. Introduction

Utilization of dielectric elastomer (DE) has increased with novel applications, among many applications soft lenses[1] and photonic crystal elastomers[2] can be mentioned. Energy harvesting from waves have also attracted major attention.[3] However most studies are still based on unoptimized elastomers, and for commercial products to enter the market, increased energy densities of the elastomers are vital. Some of the advantages of using DEs compared to other traditional transducer systems are the potential low cost, low weight, high elasticity, fast response and large strains (more than 300%).[4] So for further optimization, it is important not to compromise the favorable properties significantly.

S. S. Hassouneh, Dr. A. E. Daugaard, Dr. A. L. Skov
The Technical University of Denmark, Søltofts Plads build. 227, Lyngby 2800 Kgs., Denmark
E-mail: al@kt.dtu.dk

DEs consist of an elastomer film sandwiched between two compliant electrodes. A voltage is applied over the electrodes and the elastomer responds by deforming due to the electrostatic forces between the compliant electrodes.[5] The elastomer, therefore, contracts in thickness and expands in area. In a given electrical field (E) the mechanical response of the elastomer can be expressed by

$$-s_{Maxwell} = \frac{\varepsilon_0 \cdot \varepsilon_r \cdot E^2}{Y} = \frac{\varepsilon_0 \cdot \varepsilon_r}{Y} \cdot \left(\frac{U}{d}\right)^2 \quad (1)$$

where s is the strain, ε_0 is the vacuum permittivity, ε_r is the relative dielectric constant, Y is the Young's modulus, U is the voltage and d is the original thickness of material.[6]

The above equation takes into account the strain induced by the electrostatic field (Maxwell effect) but also the electrostriction needs to be accounted for[7,8]

$$-s_{electrostriction} = Q\varepsilon_0^2(\varepsilon_r - 1)^2\left(\frac{U}{d}\right)^2 \quad (2)$$

Macromol. Mater. Eng. 2015, 300, 542–550

DOI: 10.1002/mame.201400383

where Q is the electrostrictive coefficient. The overall strain can then be written

$$s_{tot} = s_{Maxwell} + s_{electrostriction} = M \cdot \left(\frac{U}{d}\right)^2 \quad (3)$$

where M is the apparent electrostrictive coefficient.

One way to increase the achievable strain is by increasing the working voltage, which is not desirable, since the applicability of the DE elements will be limited due to the very expensive electronics required. Another parameter that can be changed and has a great impact on the strain (as seen from Equation 1) is the thickness of the elastomer. However, for many systems, the thickness of the films is already reduced so much that it may cause processing challenges to reduce it further.[9] Therefore, to improve the actuation performance without changing the applied voltage and thickness, the most common approach is to increase the dielectric permittivity of the elastomer without increasing the Young's modulus to the same extent.

The mechanical and electrical losses of the material have an influence on the overall performance of a transducer. The losses indicate the dissipative nature of the material, i.e., energy lost to heating.[10] Therefore, the losses should be minimized such that most of the applied energy is converted into mechanical energy in actuation mode and into electrical energy in generator mode. While the mechanical losses are due to viscoelasticity, the electrical losses arise from leakage currents across the film, build-up of charges and resistive losses in the electrodes.[11]

The addition of conductive fillers in the matrix influences the dielectric losses. If the fillers are not well-dispersed, they tend to agglomerate and form conductive paths and hence increase the dielectric losses.[12] Additionally, the addition of hard fillers to soft elastomers changes the mechanical properties of the resulting composite. When the filler is added above its percolation threshold, the hard fillers form a continuous, rigid structure in the elastomer, and are thus very reinforcing. Also the interaction between filler and elastomer will strongly influence the properties of the composite.[13]

Traditionally, the research on elastomers for DE has focused on acrylics and polydimethylsiloxane (PDMS).[4] Especially, PDMS has shown promising features. PDMS elastomers have favorable properties, such as a low glass transition temperature ($T_g = -124\ ^\circ C$) and a good resistance to environmental degradation like oxygen, ozone and sunlight.[14] Another advantage of using PDMS is the possibility of tailoring the elastomer to achieve the desired elastic properties.[15,16] This is possible by controlling the stoichiometric ratio (usually denoted r) of the reactive groups and the crosslinker. For the optimization of silicone elastomers with respect to the dielectric properties, two main approaches exist, namely modification of the polymers in the network[17–20] and addition of high permittivity fillers.[4,21,22] The modification of the polymer backbone is costly due to the additional synthesis steps, but this technique causes the least destruction of the mechanical properties of the elastomers, which can be seen from swelling experiments.[18–20] Addition of conducting particles adds only slightly to the price of the resulting elastomer but does on the other hand usually introduce large changes in the mechanical properties of the resulting elastomer due to the combination of hard fillers and soft polymer network. As a new type of high-permittivity elastomers interpenetrating networks of covalent silicone and ionic components have been investigated.[22,23]

Fillers can be added and blended in a facile way, since the crosslinking reaction can be delayed by adding an inhibitor, which allows time for dispersion of fillers. Different types of fillers have been investigated to reinforce the properties of the PDMS elastomers. Conductive fillers, such as Single Walled Carbon Nanotubes,[24] Multi Walled Carbon Nanotubes,[25] graphite and carbon black[26,27], have shown enhancement in the electrical and mechanical properties. One disadvantage of adding these fillers is the increase in stiffness with increased loadings. Higher loadings of the filler in the system also result in increased tendency of electrical breakdown due to electrical percolation. For these reasons, it is not favorable to have high concentrations of conductive fillers in the system. As discussed by Stoyanov et al.,[28] subpercolative systems have the disadvantage of showing a sample thickness-dependent percolation threshold far above from what is expected. For their system consisting of carbon black in a thermoplastic copolymer, they estimated bulk properties to appear above 700 μm, which is far above the usual thicknesses of DE films (≈10–100 μm).

An alternative to the previous-mentioned fillers is expanded graphite (EG), since it is not expected to increase the stiffness substantially.[29] Natural graphite consists of multiple sheets of graphene held together by van der Waals forces, as shown in Figure 1a. By introducing the graphite to small molecules, e.g., acids[30,31] between the graphene layers followed by a rapid heating, the van der Waals bonds are broken, the acid is vaporized and the graphene sheets separates (Figure 1b). This type of graphite can be dispersed into the polymer matrix and provide an exfoliated graphite composite as sketched in Figure 1c.

The dispersion of EG into the polymer matrix is not trouble-free. The EG has a tendency to form agglomerates despite the larger distance between the graphene layers. These agglomerates have a negative impact on the electrical and mechanical properties. The polymer matrix has better compliance with the exfoliated graphite sheets than the agglomerates. A recent study was focused on dispersion methods for different loadings of EG in a 4-functional crosslinked networks.[21] The study showed that speed mixing the samples gave the best dispersion of

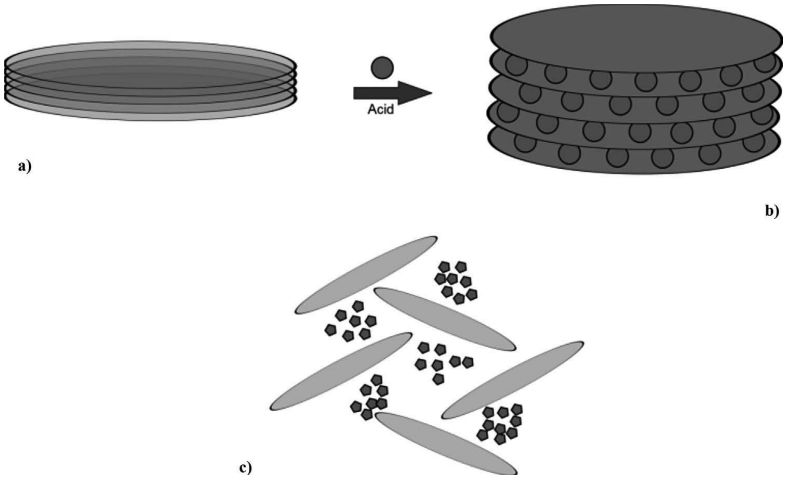

Figure 1. Different types of graphite a) natural graphite, b) expanded graphite and c) exfoliated graphite.

the EG fillers in the matrix and the percolation threshold was reached at loading of 5 wt% of EG.[21] Upon stretching of these composites it was obvious that voids were introduced around the interfaces of EG and silicone. This indicates that the network is too weak locally around the EG and thus needs reinforcement, which can be introduced by increasing the functionality of the crosslinker.[32] The purpose of this study is to facilitate successful introduction of EG into silicones without compromising the elasticity of the elastomer by adjustment of the polymer network. An 8-functional crosslinker is applied to form networks that are loaded with various concentrations of EG (2–4 wt%) to investigate the electromechanical properties of more compliant networks with less voids and thus better electromechanical properties.

2. Experimental Section

2.1. Materials and Equipment

The samples are prepared by use of PDMS (DMS-V35—49,500 g·mol^{-1}) and 8-functional crosslinker (Methylhydrosiloxane-dimethylsiloxane copolymer- HMS-301—1900–2000 g·mol^{-1}), both purchased from Gelest Inc. The inhibitor (Pt88) and the platinum catalyst (platinum cyclovinylmethyl-siloxane complex, 511) were provided by Hanse Chemie AG. The graphite used was commercially available EG TIMREX® BNB90 supplied by Timcal. The size distribution of the particles was reported by the supplier as 50% of the graphite below 36 μm and 90% below 85 μm, with a specific surface area of 28.4 m^2·g^{-1}. The benchmark silicone elastomer is commercially available Elastosil RT625 purchased from Wacker Chemie AG.

For preparation of the samples, a Speedmixer™ is used. The Speedmixer™ from Flack Tek Inc. is a Dual Asymmetric Centrifuge (DAC) 10 FVZ-K, which operates in the interval from 300–3500 rpm. The preparation of thin films was performed on an Elcometer 4340 automatic film applicator with a gap of 200 μm leading to film thicknesses of ≈120–150 μm. The rheological measurements were carried out on a controlled stress rheometer (AR2000) from TA Instruments and the samples had a diameter of 25 mm and a thickness of 1 mm.

The dielectric permittivity measurements were carried out on the ARES-G2 rheometer with the Dielectric Thermal Analysis accessory from TA Instruments. The diameter of electrodes was 25 mm.

An in-house-built device was used for measuring the actuation of the samples. A sample (60 mm * 20 mm) was fixed on frames and an area of 20 mm * 20 mm was smeared with carbon grease. Conductive electrode tape was attached to the sample, in contact with the carbon grease, to make contact to the high voltage AC amplifier. The sample is mounted with the clamps on a moveable stage controlled by a c-863 DC motor. The top clamp has a 1 kg load cell attached to measure the force the film exert when actuated at different applied voltages. The measurements were carried out at various applied voltages in the interval 1–5 kV and the samples were subjected to a 10% prestretch. Samples were actuated until electromechanical breakdown.

To measure the electrical breakdown strength, an in-house-built device based on international standards (IEC 60243-1 (1998) and IEC 60243-2 (2001)) was used. The sample thicknesses were measured with a digital thickness gage (Diesella A/S, Denmark). The sample was placed between two spherical electrodes, where the electrodes were set accordingly with a micrometer stage and gauge. To ensure good contact between the sample and the electrodes, an indent of less than 5% was added and the breakdown strength was measured at the point of contact. The sample is measures at 12 points and an average of the measurements are indicated as the breakdown strength of the sample.

The electrical breakdown strength was then measured with an increase in the applied voltage (50–100 V/step) at a rate of 0.5–1 steps/s.[32]

2.2. Mixing Procedure

The process of preparing the samples was simplified by making premixes. Premix A contained vinyl-terminated PDMS (DMS-V35, 49.67 g, 2 mmol end groups) and 8-functional crosslinker (Methylhydrosiloxane-dimethylsiloxane copolymer- HMS-301, 1.72 g, 6 mmol reactive groups) and Premix B contained the vinyl-terminated PDMS (DMS-V35, 50 g, 2.02 mmol end groups) and the platinum catalyst (platinum cyclovinylmethyl siloxane complex (511), 2.04 mg). The inhibitor was added to Premix A to allow sufficient time for thorough mixing, as well as coating, without significant onset of crosslinking.

Premix A and B were combined in a Speed Mixer cup and the EG was added in various concentrations (2–4 g depending on the desired concentration [wt%]). The samples were mixed for 5 min at 2,750 rpm. The sample was then poured in a mold or coated on a release liner and cured in the oven for 14 h at 80 °C. Samples were prepared with different concentrations of EG (2, 3 and 4 wt %) in 1 mm and 200 μm thick films.

3. Results and Discussion

PDMS samples were prepared with different concentrations of EG by speed mixing samples to obtain well-dispersed samples. To ensure a good mixing of the catalyst and crosslinker into the PDMS precursor, premixes are prepared, which simplify the process, as well as allowing for storage of premixes.[33] It was previously shown that speed mixing was an efficient way to disperse EG in silicones.[21]

3.1. Morphological Analysis

The morphology of cured samples from mechanically mixing and speed mixing, respectively, is shown in Figure 2.

The mechanically mixed elastomer contains big agglomerates of the EG fillers. The mechanical mixing is not sufficient to break the agglomerates and thereby get a good micro-scale dispersion of the fillers in the PDMS matrix. By speed mixing the sample, the agglomerates are broken to a larger extent and the EG fillers are better dispersed throughout the sample as illustrated in Figure 2b. The particle size varies strongly for the mechanically mixed samples, where agglomerates of length ≈200 μm are rather common, to the speed mixed samples, where the largest agglomerates are of the order of 50 μm.

3.2. Mechanical Properties

The mechanical properties for the samples with different loadings and the benchmark sample (Elastosil RT625) are compared and illustrated in Figure 3. Small amplitude oscillatory shear is used to investigate the mechanical properties and the fillers influence on the network.

Figure 3 shows that the storage moduli decrease with increasing loading of the EG fillers. The storage moduli for the 2 and 3% loaded samples are comparable with the benchmark silicone elastomer Elastosil RT625 within +/−10%, which is within common uncertainty on the determination of G′ for soft elastomers. The sample with a concentration of 4% has a significantly lower storage modulus (≈ a factor of 2). This is not what is commonly encountered in composites of thermoplastic polymers, which usually show increases in G′ with loading. Seen from the perspective of the actuation equation (Equation 1) the decreased storage modulus is favorable, since $Y = 3G'$ ($\omega \rightarrow 0$) and thus increased actuation should be obtained solely from the decrease in G'. However, this behavior indicates that major network destruction is taking place.

The increased interfacial area with increased loading could impose a steric hindrance and a reduction of mobility in the matrix, which is well known for nano-composites. This would result in a slower or incomplete reaction and especially affect systems with an already reduced volume

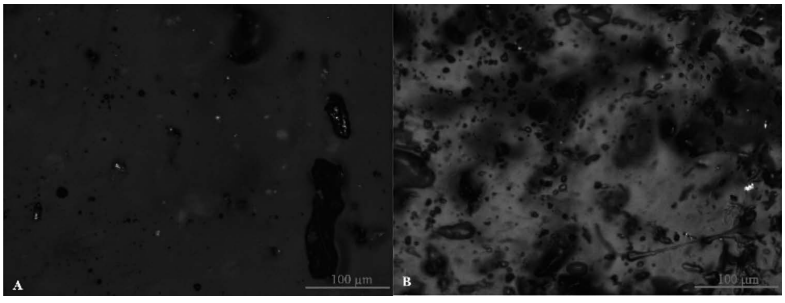

Figure 2. Optical microscope images of the dispersion of EG in a mechanically mixed sample (A) and a speed mixed sample (B).

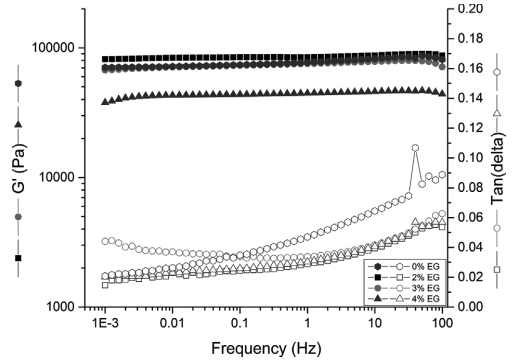

Figure 3. Linear viscoelastic properties of PDMS-V35 network with different loadings of EG compared to the unfilled benchmark elastomer Elastosil RT625.

as in a thin film system. In a similar manner, the increased surface area of the filler in the well-dispersed reaction media could interact with the platinum catalyst and inhibit the reaction, which again would result in a slower or incomplete reaction. The observed reduction in moduli with improved dispersion of the filler could also be explained based on the steric hindrance around the particles, which would result in local internal 2-dimensional (2D) curing. 2D curing is in contrast to traditional 3D curing of the elastomer in the bulk. At the surface, the dynamics of the crosslinker is strongly reduced since the crosslinker relies on self-diffusion rather than on reptation.[34] Furthermore, the number of reactive sites surrounding the interface crosslinker is reduced by approximately a factor of 2 and, thus, the crosslinker becomes more susceptible to participating in loop formations or simply not reacting. Both phenomena ultimately lead to the crosslinker becoming a chain extender and, thus, decrease the effective crosslinking concentration. For the 4-functional crosslinker, the formation of one loop causes the loss of crosslinking capability, as well as two unreacted sites have the same effect. For the 8-functional crosslinker, 3 times as many occurrences are required.

This surface phenomenon is very often observed at a macroscopic level for Pt-catalyzed silylation room temperature vulcanized silicone (RTV), where the surface of a sample may feel sticky or greasy, whereas the bulk is completely nonsticky and fully cured. If this phenomenon is taking place, it would be expected that increased dispersion of the filler would result in a reduction in storage moduli of the samples and formation of small voids in the system.

In a previous study, a 4-functional crosslinker was used.[21] Upon comparison of the 8-functional system with the previous studied 4-functional crosslinked system, it can be seen that the storage moduli are lower for the 8-functional crosslinked system with the 3% and 4% EG-loaded samples and higher for the 2% EG loaded sample. This behavior can be explained by better incorporation of the 3% and 4% EG in the 8-functional network compared to the 4-functional network. For the 2% loaded samples, dispersion is good in both types of networks and the 8-functional network, thus, has the highest elastic modulus as predicted by classical network theories.

Table 1 shows the storage and loss moduli at 0.01 Hz and the viscous loss of each network.

The greatest viscous loss can be seen for the 3% EG-loaded sample, while 2 and 4% have similar viscous losses as that of Elastosil RT625. This behavior can be explained by higher tendency to 2D curing and, thus, decreased G′ with loading.

In an earlier study,[21] a 4-functional crosslinker was used for crosslinking of the matrix. The study showed that the relative viscous dissipation between 100 and 0.01 Hz was of the order of 10, higher than what is reported here. This is a result of 2D curing and the occurrence of voids in the matrix. By using an 8-functional crosslinker, this phenomenon is eliminated and the matrix is improved.

3.3. Dielectric Properties

The dielectric permittivity is measured for all DMS-V35 samples loaded with EG (2–4 wt%) and the pure Elastosil RT625 on the ARES G2 with dielectric thermal analysis fixture. Figure 4 illustrates the dielectric measurements for the EG loaded samples with different loadings of EG and RT625 (0 wt% EG).

The figure shows that by increasing the loading of EG the permittivity increases as expected. The permittivity for the 2 and 3 wt% loaded samples and RT625 are almost constant over the whole frequency range, whereas the permittivity for the 4 wt% loaded sample is decreasing with increasing frequency, showing a strong tendency to Maxwell polarization at low frequencies.

In a previous study,[21] where the PDMS matrix was vulcanized with a 4-functional crosslinker, the permittivity was measured to 8.6 for the 4% EG loaded sample. This increase in permittivity was caused by the large surface area of the particles being active. For the 8-functional crosslinked system, the dielectric permittivity was measured to 12,

Table 1. Mechanical properties at room temperature and at 0.01 Hz.

Sample	G′ [kPa]	G″ [kPa]	Tan δ
2% EG	84	1.9	0.023
3% EG	71	2.6	0.037
4% EG	43	1	0.023
RT625	72	1.9	0.026

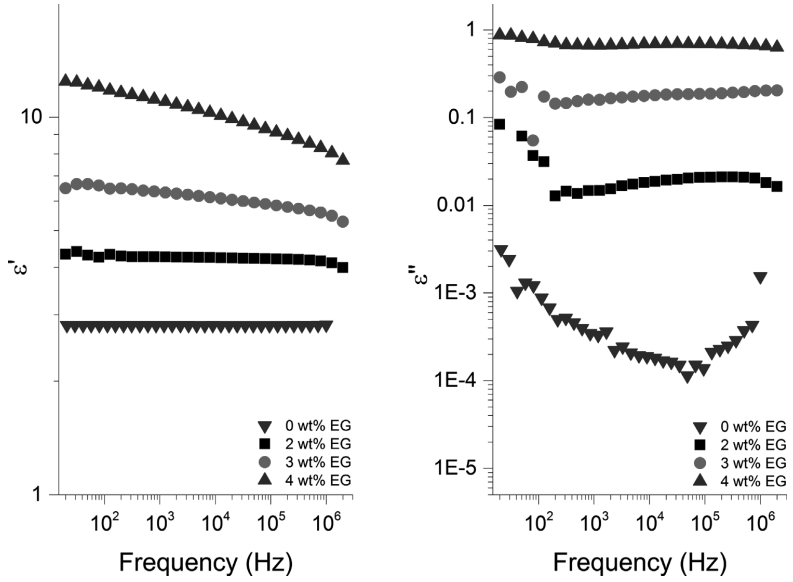

Figure 4. Dielectric permittivity measurements for the different loadings of EG and Elastosil RT 625 at 21 °C.

which is a 40% increase to the 4-functional crosslinked system and a 375% increase to the commercially available system Elastosil RT625. This increase in the dielectric permittivity could be caused by the improved matrix facilitating better distribution, as well as the crosslinking density will determine the mobility in the network.

The electrical breakdown strengths are measured for the different loadings and compared to the benchmark silicone elastomer, which are depicted in Figure 5. The error bars for each sample measurement are shown as vertical lines.

The figure shows an increase in the breakdown strength with increasing loadings of EG. The breakdown strength was 40 $V \cdot \mu m^{-1}$, 41 $V \cdot \mu m^{-1}$ and 48 $V \cdot \mu m^{-1}$ for the 2% EG, 3% EG and 4% EG loaded samples, respectively. However, in comparison with the benchmark, the breakdown strength (81 $V \cdot \mu m^{-1}$) decreases with a factor 2. This decrease is due to a combination of increased conductivity, changed morphologies (the benchmark material contains non-conductive silica fillers which reinforce the material) and mechanical properties when EG is added to the otherwise homogeneous silicone elastomer.

The standard deviation on the reference film is +/− 7 $V \cdot \mu m^{-1}$, which is rather large but not uncommon when several breakdown phenomena are occurring simultaneously.[35] For the elastomers with EG, the standard deviations drop to +/− 2 $V \cdot \mu m$, which indicates that there is one single phenomenon causing the electrical breakdown. The samples with unoptimized network showed strong dependence on the location of the electrode when testing for breakdown strength such that the variation in the determination of the breakdown strength was very large with data scattered in between 20 and 50 $V \cdot \mu m$, indicating the very non-homogeneous distribution of EG. These samples were, therefore, not suitable candidates for dielectric elastomers as they would fail instanteneously

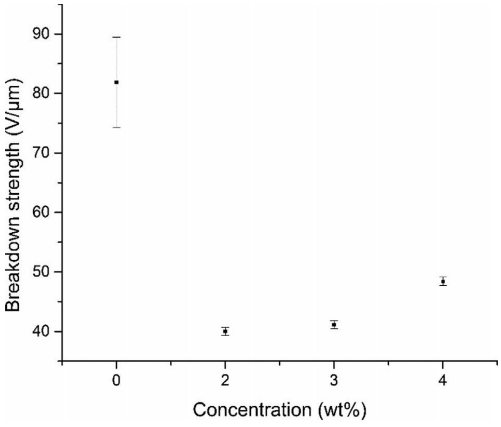

Figure 5. Breakdown strength of the various composites.

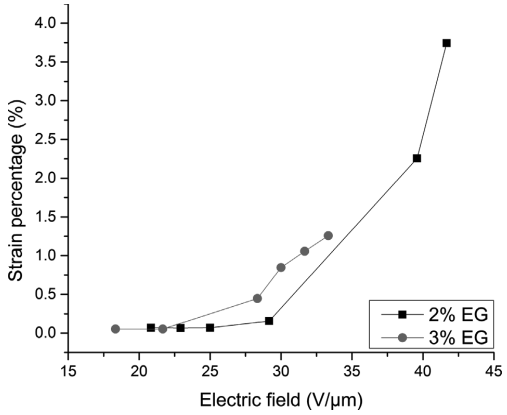

Figure 6. Sample actuation curves for the 2% and 3% loadings of EG.

when the entire elastomer was subjected to an electrical field rather than just single points.

3.4. Electromechanical Properties

The actuation performance of the materials with different loadings of EG was measured on 120–150 μm thick films. The thicknesses were chosen to be above the largest particles size as to avoid single-particle short-circuiting. Different voltages (1–5 kV) were applied to 10% prestretched samples and the force was measured. The prestretch was introduced to soften the elastomer slightly, as well as to avoid uncertainty on the zero-stress state of the elastomer, and thus reduce measurement uncertainties due to wrinkling etc.

The electric field as a function of the strain is illustrated in Figure 6. The figure shows, as expected, that the strain increases slightly faster for 3% EG with increasing electric field. For the 2% sample, there is a good agreement between the results from the electrical breakdown measurements (Figure 5), whereas for the 3% sample the coupled electromechanical breakdown strength is lowered with ≈8 V·μm, which indicates that the electrical breakdown strength decreases with alignment of the EG plates.

The measured actuation performance is compared with the predicted actuation, which is illustrated in Figure 7. The predicted actuation performance is calculated from the measured dielectric permittivity and Young's modulus using Equation (1). Figure 6 shows that the actual measured strains are not consistent with the predicted measurements. This can be attributed to heating arising from both electrical and mechanical losses leading to an increased leakage current before the electrical field becomes so large that it exceeds the leakage. A recent study of Zakaria et al.[36] showed that even changes of 10 °C could potentially lead to detrimental behavior of dielectric elastomers. Furthermore, air voids may be introduced upon stretching leading to lower actuation. The apparent electrostrictive coefficient, *M*, has been determined, but since there seems to be no actuation of the elastomer composites before a certain threshold value, the values were not predictive.

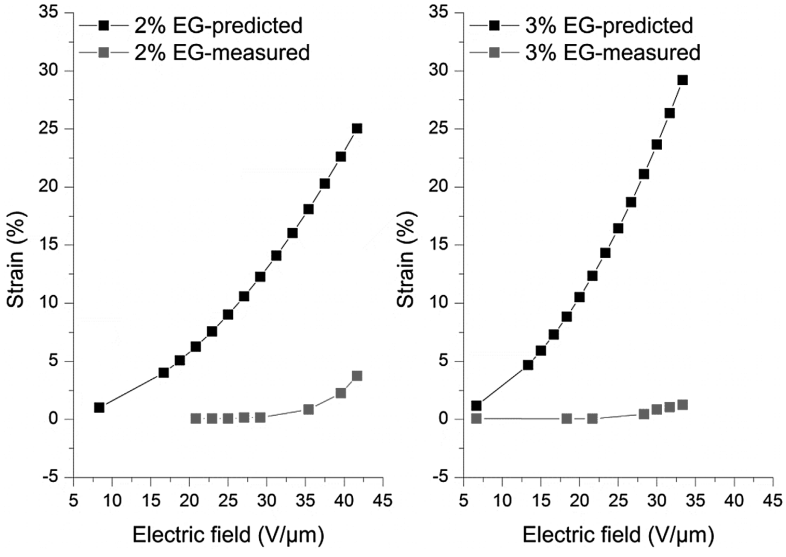

Figure 7. Experimental versus theoretical actuation of composites at room temperature.

This difference between the predicted and measured actuation at higher electric field is approximately a factor of 5 for the 2% EG loaded samples and approximately 30 for the 3% EG loaded sample. The difference in the measured and predicted values can be caused by a leakage current, which indicates that the material is not a perfect insulator and has some conductivity. Breakdown may also be facilitated by voids at the interfaces upon stretch, where the local deformation may be anisotropic due weak interfacial forces between EG sheets and silicone matrix.

The dimension of the EG sheets are of the order of 60 μm (as determined from the optical images in Figure 2b). For comparison, the end-to-end distance of the polymer applied in this study is calculated.[37] It is assumed that the PDMS polymer chain has an average molecular weight $M = 50\ kg{\cdot}mol^{-1}$, the average bond length is 1.5 Å and that the polymer chain can be described by a simple random walk with step length of the repeat unit [-Si-(CH3) 2-O] ($M_o = 74\ g{\cdot}mol^{-1}$). The number of repeat units is $N = M/M_o = 50{,}103/74 = 677$ and the length of one repeat unit consisting of two bonds is $b = 2 * 1.5\ Å = 3Å$. The (random walk) end-to-end distance is $R = \sqrt{N} * b = \sqrt{677} * 3 = 78$. The area of an EG plate is assumed to be 60 μm times 60 μm. From these calculations, it is obvious that the 2D effect is rather significant, since the area of one EG facilitates approximately $6 * 10^7$ 2D crosslinks. This large number indicates the significance of the local environment of the interface between elastomer and EG. Therefore, it is important that the crosslinker provides the possibility of forming a 2D network at the surface with similar stress-releasing properties as the matrix such that stress-induced voids are minimized. The 8-functional crosslinker facilitates a stronger network in the surface since the crosslinker does not need to be fully reacted in order to act as a crosslinker, whereas for the 4-functional crosslinker is acting as chain extender if two of the reactive sites are participating in reaction with the same end-functionalized PDMS, i.e., a loop, or if the local environment allows for two reactions only.

4. Conclusion

The silicone matrix is attempted improved by using an 8-functional crosslinker instead of a previous studied 4-functional crosslinked system.[21] The samples are loaded with different concentrations (2–4 wt%) of EG to investigate the influence of EG on the electromechanical properties.

The mechanical properties were investigated and showed that the material got softer with increasing loadings of EG. This is explained by the 2D curing taking place at the interface between silicone and EG. In contrast to the previously reported 4-functional crosslinker, the 8-functional crosslinker facilitated better dispersion, as well as the electromechanical properties were improved since the interfaces were better crosslinked and the void formation upon stretching was reduced.

It was shown that the dielectric permittivity was increased with increasing loadings of EG. The dielectric permittivity for the 4% EG 8-functional crosslinked system was increased with 40% to a value of 12 compared to the 4% EG loaded 4-functional crosslinked system and a 375% increase compared to Elastosil RT625.

The electrical breakdown strength increases with increasing loadings of EG, where the breakdown strength was 40 V·μm for the 2% EG, 41 V·μm for the 3% EG and 48 V·μm for the 4% EG sample. Compared to the benchmark, the breakdown strength decreases with a factor 2, but this was expected since the benchmark is filled with non-conductive silica particles.

The predicted actuation was calculated from the measured dielectric permittivity and Young's modulus and compared with the measured actuation. The measured actuation was a factor of ≈5 lower than the predicted measurements for the 2% EG-loaded samples and a factor of ≈30 for the 3% EG-loaded sample.

Acknowledgments: The authors would like to thank the Danish Agency for Science and InnovationsFonden for financial support. Sindhu Vudayagiri is acknowledged for her help with the actuation measurements.

Received: November 4, 2014; Revised: January 2, 2015; Published online: February 4, 2015; DOI: 10.1002/mame.201400383

Keywords: capacitance; expanded graphite; electrical properties; PDMS

[1] F. Carpi, G. Frediani, S. Turco, D. De Rossi, *Adv. Funct. Mater.* **2011**, *21*, 4152.
[2] Q. Zhao, A. Haines, D. Snoswell, C. Keplinger, R. Kaltseis, S. Bauer, I. Graz, R. Denk, P. Spahn, G. Hellmann, J. J. Baumberg, *Appl. Phys. Lett.* **2012**, *100*, 101902.
[3] S. J. A. Koh, C. Keplinger, T. Li, S. Bauer, Z. Suo, *IEEE/ASME Trans. Mechatronics* **2011**, *16*, 33.
[4] P. Brochu, Q. Pei, *Macromol. Rapid Commun.* **2010**, *31*, 10.
[5] X. Zhang, C. Löwe, M. Wissler, B. Jähne, G. Kovacs, *Adv. Eng. Mater.* **2005**, *7*, 361.
[6] R. Pelrine, R. Kornbluh, Q. Pei, J. Joseph, *Science* **2000**, *287*, 836.
[7] Z. Suo, X. Zhao, W. Greene, *J. Mech. Phys. Solids* **2008**, *56*, 467.
[8] B. Guiffard, L. Seveyrat, G. Sebald, D. Guyomar, *J. Phys. D. Appl. Phys.* **2006**, *39*, 3053.
[9] S. Vudayagiri, M. D. Junker, A. L. Skov, *Polym. J.* **2013**, *45*, 871.
[10] R. Kornbluh, R. Pelrine, Q. Pei, S. Oh, J. Joseph, *Proc. SPIE* **2000**, 3987.
[11] R. D. Kornbluh, R. Pelrine, H. Prahlad, A. Wong-Foy, B. McCoy, S. Kim, J. Eckerle, T. Low, *Proc. SPIE* **2011**, *7976*, 797605.

[12] M. Molberg, D. Crespy, P. Rupper, F. Nüesch, J-A. E. Månson, C. Löwe, D. M. Opris, *Adv. Funct. Mater.* **2010**, *20*, 3280.
[13] J. S. Bergström, M. C. Boyce, *Rubber Chem. Technol.* **1999**, *72*, 633.
[14] M. Kujawski, J. D. Pearse, E. Smela, *Carbon* **2010**, *48*, 2409.
[15] A. L. Larsen, P. Sommer-Larsen, O. Hassager, *Proc. SPIE* **2004**, *5385*, 108.
[16] S. M. G. FrankÌr, M. K. Jensen, A. G. Bejenariu, A. L. Skov, *Rheol. Acta* **2012**, *51*, 559.
[17] C. Racles, M. Cazacu, B. Fischer, D. M. Opris, *Smart Mater. Struct.* **2013**, *22*, 104004.
[18] F. B. Madsen, A. E. Daugaard, S. Hvilsted, M. Y. Benslimane, A. L. Skov, *Smart Mater. Struct.* **2013**, *22*, 104002.
[19] F. B. Madsen, I. Dimitrov, A. E. Daugaard, S. Hvilsted, A. L. Skov, *Polym. Chem.* **2013**, *4*, 1700.
[20] B. Kussmaul, S. Risse, G. Kofod, R. Waché, M. Wegener, D. N. Mccarthy, H. Krüger, R. Gerhard, *Adv. Funct. Mater.* **2011**, *21*, 4589.
[21] A. Egede Daugaard, S. S. Hassouneh, M. Kostrzewska, A. G. Bejenariu, A. L. Skov, *Proc. SPIE* **2013**, *8687*, 868729.
[22] L. González, L. Yu, S. Hvilsted, A. L. Skov, *RSC Adv.* **2014**, *4*, 36117.
[23] L. Yu, L. B. Gonzalez, S. Hvilsted, A. L. Skov, *Proc. SPIE* **2014**, *9056*, 90560C.
[24] P. Zylka, *Prz. Elektrotechniczny* **2010**, *86*, 39.
[25] Z. Zhang, S. Sun, L. Liu, K. Yu, Y. Liu, J. Leng, *Proc. SPIE* **2009**, *7493*, 749315.
[26] M. Kujawski, J. Pearse, E. Smela, *Proc. SPIE* **2010**, *7642*, 76420R.
[27] G-H. Chen, D-J. Wu, W-G. Weng, W-L. Yan, *J. Appl. Polym. Sci.* **2001**, *82*, 2506.
[28] H. Stoyanov, D. Mc Carthy, M. Kollosche, G. Kofod, *Appl. Phys. Lett.* **2009**, *94*, 232905.
[29] M. G. Urdaneta, R. Delille, E. Smela, *Adv. Mater.* **2007**, *19*, 2629.
[30] M. Li, Y. G. Jeong, *Macromol. Mater. Eng.* **2011**, *296*, 159.
[31] R. Wissert, P. Steurer, S. Schopp, R. Thomann, R. Mülhaupt, *Macromol. Mater. Eng.* **2010**, *295*, 1107.
[32] M. Y. Benslimane, H-E. Kiil, M. J. Tryson, *Polym. Int.* **2010**, *59*, 415.
[33] A. L. Larsen, K. Hansen, P. Sommer-Larsen, O. Hassager, A. Bach, S. Ndoni, M. Jørgensen, *Macromolecules* **2003**, *36*, 10063.
[34] P. Cicuta, I. Hopkinson, *Europhys. Lett.* **2004**, *68*, 65.
[35] S. Vudayagiri, S. Zakaria, L. Yu, S. S. Hassouneh, M. Benslimane, A. L. Skov, *Smart Mater. Struct.* **2014**, *23*, 105017.
[36] Z. Shamsul, P. H. F. Morshuis, B. Mohamed, K. V. Gernaey, A. Ladegaard, *Proc. SPIE* **2014**, *9056*, 90562V.
[37] M. Doi, *Introduction to Polymer Physics*, Oxford University Press, New York **1996**.

The Danish Polymer Centre
Department of Chemical and Biochemical Engineering
Technical University of Denmark
Søltofts Plads, Building 227
DK-2800 Kgs. Lyngby
Denmark

Phone: +45 4525 6801
Web: www.dpc.kt.dtu.dk

ISBN : 978-87-93054-75-2